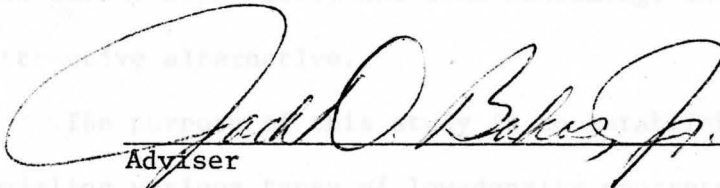


SCALE MODEL STUDY OF LOW-DENSITY
CONCRETE IMPACT ATTENUATORS

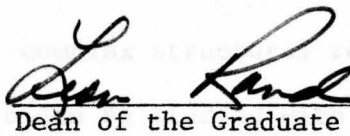
by

Robert W. Rimko

Submitted in Partial Fulfillment of the Requirements
for the Degree of
Master of Science in Engineering
in the
Civil Engineering
Program



Adviser 3/5/77
Date



Dean of the Graduate School 3/9/77
Date

YOUNGSTOWN STATE UNIVERSITY

March, 1977

ABSTRACT

SCALE MODEL STUDY OF LOW-DENSITY
CONCRETE IMPACT ATTENUATORS

Robert W. Rimko

Master of Science in Engineering

Youngstown State University, 1977

The series of events taking place during an automobile-impact attenuator collision is extremely complex. The response of the attenuator upon impact is dependent on a large number of variables including vehicle impact velocity, weight and angle of incidence.

Current research depends heavily on full-scale experiments to determine the crashworthiness of an attenuator design. This approach can become both costly and time consuming, making scale modeling an attractive alternative.

The purpose of this study is to establish the feasibility of modeling various types of low-density concrete and to show by example that the complex structural response of an automobile-impact attenuator collision can be studied with scale models.

ACKNOWLEDGEMENTS

The author would like to thank Dr. Jack D. Bakos, Jr., for the opportunity to work on this project. Special thanks go to Jim Eckert, Mike Repetski, Phil Krupa and Dave Vanaman for their time and efforts, and to Wylma Evans for typing the manuscript.

LIST OF TABLES. viii

CHAPTER I. INTRODUCTION. 1

CHAPTER II. SCALING LAWS AND IMPACT TESTS. 6

 2.1 Introduction. 6

 2.2 Similarity. 10

 2.3 Scale Model Vehicle Design. 13

 2.4 Scaling Effects of Lightweight Components. 31

 2.5 Scaling Effects of Crash Cushion Shape. 43

 2.6 Model Barrier Fabrication. 64

CHAPTER III. SCALE MODEL IMPACT TEST FACILITY. 64

CHAPTER IV. IMPACT TEST RESULTS AND DISCUSSION. 74

CHAPTER V. CONCLUSIONS AND RECOMMENDATIONS. 97

APPENDIX A. Least Squares Regression. 100

APPENDIX B. High Speed Camera Specifications. 101

APPENDIX C. Raw data from High Speed Camera. 105

LIST OF REFERENCES. 106

TABLE OF CONTENTS

	PAGE
ABSTRACT.	ii
ACKNOWLEDGEMENTS.	iii
TABLE OF CONTENTS.	iv
LIST OF FIGURES	v
LIST OF TABLES.	vii
CHAPTER	
I. INTRODUCTION.	1
II. SCALING LAWS AND PRELIMINARY TESTS.	6
2.1 Introduction.	6
2.2 Similitude.	10
2.3 Scale Model Vehicle Design.	13
2.4 Scaling Effects of Lightweight Concrete	31
2.5 Scaling Effects of Crash Cushion Shape.	43
2.6 Model Barrier Fabrication	64
III. SCALE MODEL IMPACT TEST FACILITY.	69
IV. IMPACT TEST RESULTS AND DISCUSSION.	74
V. CONCLUSIONS AND RECOMMENDATIONS	97
APPENDIX A. Least Squares Regression.	100
APPENDIX B. High Speed Camera Specifications.	101
APPENDIX C. Raw data from High Speed Camera	105
LIST OF REFERENCES.	109

2.70 Prototype and Model Modules.	32
2.21 Static Testing of Prototype Module	37
2.22 Static Testing of Model Module	37
2.23 Force-Displacement Curve for Dynamic Module	40
2.24 Force-Displacement Curve for Module-A Module	42

LIST OF FIGURES

FIGURE	PAGE
1.1 Crash Cushion Configuration.	1
2.1 Vehicle Weight vs. Deceleration.	8
2.2 Theoretical Barrier Force-Deformation Relationship . . .	9
2.3 Average Automobile Weights	15
2.4 Vehicle Center of Gravity.	21
2.5 Basic Model Vehicle Form	26
2.6 Scale Model Dimensions	27
2.7 Wheel Reverse Brake.	29
2.8 Scale Model Vehicles	30
2.9 Scale Model Vehicles	30
2.10 Dycon IV Concrete Matrix	34
2.11 Dycon IV Cubes	34
2.12 Apparatus for Static Compression Testing	35
2.13 Crash Cushion With Cylindrical Voids	45
2.14 Crash Cushion With Rectangular Voids	46
2.15 Empirical Design of Crash Cushion.	48
2.16 Module Construction.	52
2.17 Module Construction.	52
2.18 Module Construction.	53
2.19 Module Construction.	53
2.20 Prototype and Model Modules.	55
2.21 Static Testing of Prototype Module	57
2.22 Static Testing of Model Module	57
2.23 Force-Displacement Curve for Dycon-2 Modules	60
2.24 Force-Displacement Curve for Perlite-4 Modules	63

LIST OF FIGURES (Continued)

FIGURE	PAGE
2.25 Exploded View of Scale Model Crash Cushion.	66
2.26 Completed Scale Model Crash Cushion	67
2.27 Force-Displacement Curve for Cast and Bonded Dycon-2 Scale Model Modules	68
3.1 Scale Model Impact Test Facility.	71
3.2 Crash Cushion and Vehicle in Place Before Test.	71
3.3 Computer Program to Analyze Film Data	73
4.1 Dycon-2 Barrier Impacted by "2,000 Pound" Vehicle	74
4.2 Tabulated Impact Test Data.	76
4.3 Impact Test Results	80
4.4 Impact Test Results	81
4.5 Impact Test Results	82
4.6 Impact Test Results	83
4.7 Impact Test Results	84
4.8 Impact Test Results	85
4.9 Impact Test Results	86
4.10 Impact Test Results	87
4.11 Prototype and Scale Model Test Vehicles	93
4.12 Sequential Photographs of Impact Tests.	94
4.13 Sequential Photographs of Impact Tests.	95
4.14 Summary of Impact Test Data	96
5.1 Dimensions for a Dycon-2 Crash Cushion Module	99

LIST OF TABLES

TABLE	PAGE
2.1 Cauchy Similitude Laws.	12
2.2 Typical Vehicle Dimensions.	17
2.3 Vehicle Parameter Averaging	19
2.4 Composite Car Dimensions.	20
2.5 Composite Center of Gravity	22
2.6 Weight/Scale Relationships.	22
2.7 Scale Model Dimensions.	28
2.8 Average Values for Energy Absorption.	36
2.9 Absorbed Energy Vs. Volume.	40
2.10 Change in Slope	41
2.11 Forecasted Vs. Extrapolated Energy Absorption Values .	42
2.12 Load Vs. Displacement Values for Dycon-2 Modules. . .	58
2.13 Average Load Vs. Displacement Values for Dycon-2 Modules	59
2.14 Load Vs. Displacement Values for Perlite-4 Modules. .	61
2.15 Average Load Vs. Displacement Values for Perlite-4 Modules	62
4.1 TABULATED Scale Model Test Results.	77

FIGURE 1.1
CRASH CIRCUMFERENCE COMPARISON

CHAPTER I
INTRODUCTION

Collision with stationary objects has been found to be the leading source of fatalities on the Interstate Highway system and other freeways. Gore areas of freeway off-ramps, in which can be found signposts, bridge rail end posts, and other rigid structures, have been particularly troublesome. Various types of energy-absorbing barriers have been developed and installed at selected gore locations across the country. The general configuration of these gore area barriers can be seen in Figure 1.1.

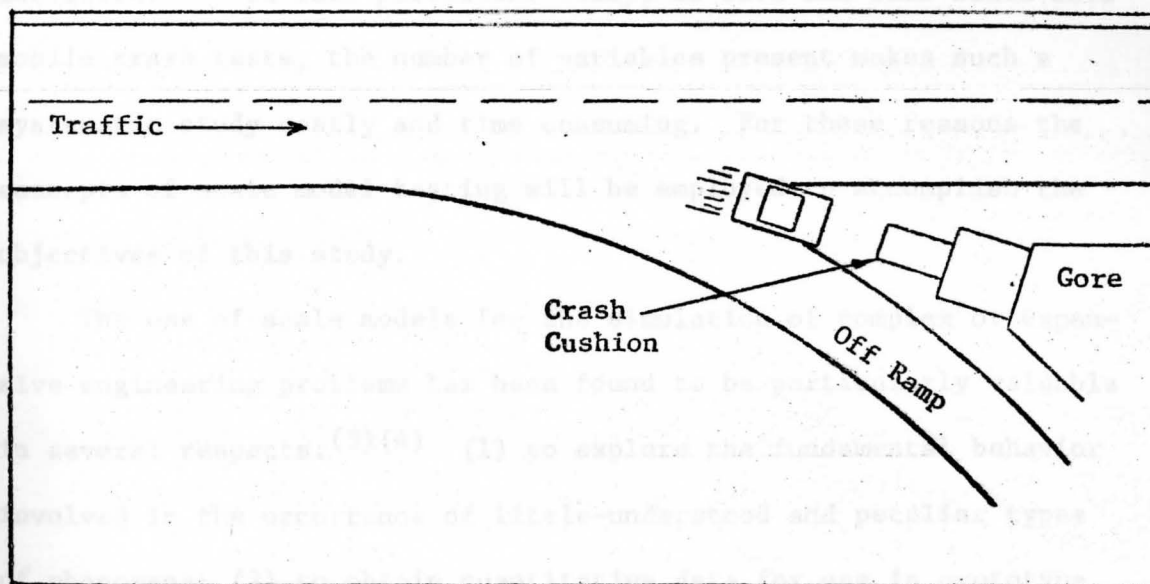


FIGURE 1.1
CRASH CUSHION CONFIGURATION

One concept that has not been given a thorough investigation is the use of lightweight concrete in the construction of energy-absorbing barriers.

A recent study^{(1)*} completed by Dr. Jack D. Bakos, Jr., and sponsored by the Ohio Department of Transportation in cooperation with the Federal Highway Administration, established the possibility of using low-density concretes such as foam concrete, perlite concrete and polystyrene concrete as energy absorbing materials utilized in an attenuator system. The feasibility of utilizing vehicle crash cushions constructed of lightweight vermicular concrete has also been demonstrated through a series of full scale vehicle impact tests on prototype installations conducted at the Texas Transportation Institute.⁽²⁾ In this particular study, as with all full scale automobile crash tests, the number of variables present makes such a systematic study costly and time consuming. For these reasons the concepts of scale model testing will be employed to accomplish the objectives of this study.

The use of scale models for the simulation of complex or expensive engineering problems has been found to be particularly valuable in several respects:⁽³⁾⁽⁴⁾ (1) to explore the fundamental behavior involved in the occurrence of little-understood and peculiar types of phenomena; (2) to obtain quantitative data for use in prototype design problems, particularly when mathematical theory is overly complex or non-existent; and (3) to obtain quantitative and qualitative data with minimum expense and effort.

*Number in parenthesis indicates reference cited.

The application of the techniques of scale modeling to the study of low-density concrete crash cushions would eliminate the need for sophisticated instrumentation as well as the need for large test facilities as required for full size automobile crash experiments. The scale model experiments can be conducted in a laboratory under well controlled test conditions and the same experiment can be repeated as often as necessary to check the reproducibility of the results.

Two general types of dynamic modeling techniques are recognized.⁽⁵⁾ Geometrically similar modeling is widely used and its technique is well developed due to less complexity in relating the model and the full scale prototypes. Wind-tunnel tests of aircraft and aerospace vehicles are well known applications of this technique. A skew model is a distorted model of a prototype that gives a possible amplified response of a portion of a structure. Skew modeling is generally less popular in model testing because of inherent complexities in the basic model-to-prototype relationship, such as less accuracy in predicting the prototype's dynamic behavior from the model's. A geometrically similar model is, therefore, recommended for the attenuator prototype design.

Several investigators have resorted to scale model testing of energy absorbing barriers. Fay and Wittrock⁽⁶⁾ of the Denver Research Institute, University of Denver, conducted a scale model test of the Texas Barrel Barrier in order to demonstrate the great utility of scale modeling in a study of energy absorbing highway barriers. The test was restricted to a head-on collision of a model car impacting

an array of scale model 55 gallon drums. Test results were compared to the results of the actual test conducted by the Texas Transportation Institute. The results of the scale model tests were found to agree very well with the results from the full scale test that was modeled. It was concluded from their study that the same techniques may be applied to barriers of any design with the ultimate goal of designing a barrier that is optimized with regard to overall efficiency including the cost of materials and labor to build and install the barrier. It should be noted that no attempt was made in this study to scale the wall thickness of the model 55 gallon drum, i.e., the prototype.

In another study conducted at the Denver Research Institute by Fay and Kaplan,⁽⁷⁾ a new concept in energy absorbing highway buffers was developed and tested with scale models. The buffer was made of corrugated metal elements that deformed plastically on impact and absorbed the energy of the impacting vehicle. Scale model testing was found to be a valuable tool in that the tests were conducted for a small fraction of the cost and time of full scale tests.

The objective of this study is to apply the techniques of scale modeling to the design and analysis of low-density concrete crash cushions and to ascertain the degree to which a full scale crash barrier would minimize the hazards created by gore area structures and other fixed roadside objects.

This scale model study is, however, limited to head-on collisions with vehicles of varying weight and impact velocities. No side angle impact studies will be attempted.

Consideration is also given in this study to full size barrier casting and handling during erection and replacement.

1.2 Introduction

The purpose of this study is to provide the designer with criteria for full size crash cushions will be used. The top two important requirements of a barrier system are structural strength and occupant safety. Thus, a crash cushion must determine an impacting vehicle in such a manner that occupants restrained by seat belts can survive, preferably uninjured. These two requirements are interdependent and must be considered simultaneously in order to achieve an optimal barrier performance. For instance, it may be necessary to reduce the rigidity of a barrier system in order to lessen the severity of an impact, thereby improving safety.

To aid the designer, the Federal Highway Administration has set forth the following criteria for the development and analysis of crash cushions: (1) vehicle weight range, 2,000 lb. to 4,500 lb.; (2) vehicle impact speed, 30 mph; (3) impact angle, up to 25° as measured from the direction of the roadway; (4) a maximum average permissible vehicle deceleration of 32 G's, as calculated from the relationship $a_g = \frac{V^2}{2x}$ where a_g is the average vehicle deceleration, V is the vehicle impact velocity, x is the vehicle displacement after impact, and g is the acceleration due to gravity; (5) a maximum occupant deceleration onset rate of 500 G per second.

In addition, it is important that the crash cushion stop or redirect the vehicle in such a manner as to minimize any hazard to

CHAPTER II

SCALING LAWS AND PRELIMINARY TESTS

2.1 Introduction

At this point an examination of the current performance criteria for full size crash cushions will be made. The two most important requirements of a barrier system are structural strength and occupant safety; i.e., a crash cushion must decelerate an impacting vehicle in such a manner that passengers restrained by seat belts can survive, preferably uninjured. These two requirements are interdependent and must be considered simultaneously in order to achieve an optimum barrier performance. For instance, it may be necessary to reduce the rigidity of a barrier system in order to lessen the severity of an impact, thereby improving safety.

To aid the designer, the Federal Highway Administration has set forth the following criteria for the development and analysis of crash cushions: (1) vehicle weight range, 2,000 lb. to 4,500 lb.; (2) vehicle impact speed, 60 mph; (3) impact angle, up to 25 as measured from the direction of the roadway; (4) a maximum average permissible vehicle deceleration of 12 G's, as calculated from the relationship $G_a = \frac{v^2}{2gx}$ where G_a is the average vehicle deceleration, V is the vehicle impact velocity, x is the vehicle displacement after impact, and g is the acceleration due to gravity; (5) a maximum occupant deceleration onset rate of 500 G per second.

In addition, it is important that the crash cushion stop or redirect the vehicle in such a manner as to minimize any hazard to

following or adjacent traffic. Ideally, the vehicle should remain close to the barrier installation and not be directed back into the traffic stream.

The design of crash cushions is a complex task because of the seemingly conflicting performance requirements. A closer look at the chain of events occurring during impact is warranted. An automobile travelling along a highway possesses kinetic energy. This energy can be calculated from $KE = \frac{W \cdot V^2}{2 \cdot g}$ where W is the vehicle weight, g is the acceleration of gravity, and V is the vehicle velocity. Therefore, a 4,500 pound vehicle travelling at 60 mph possesses 540,000 ft.-lb. of kinetic energy. Similarly, a 2,000 lb. vehicle going 60 mph will possess 240,000 ft.-lb. of kinetic energy.

At the moment of impact, the portion of the crash cushion in direct contact with the vehicle and the vehicle itself are rapidly brought to a common velocity. When the ratio of the barrier mass activated at impact to vehicle mass is close to unity, then this common velocity is significantly different from the vehicle's impact velocity and large deceleration forces occur.⁽⁹⁾ The intensity of this deceleration force induced in the vehicle is a function of the crash cushion resisting force and the vehicle weight. From Newton's Second Law of Motion:

$$F \text{ (force)} = M \text{ (mass)} \cdot a \text{ (acceleration)}$$

substituting $M = \frac{w \text{ (weight)}}{g \text{ (gravitational acceleration)}}$

and $a = G \cdot g$

then $G = \frac{F}{W}$

Thus, for a given crash cushion force, deceleration is inversely proportional to vehicle weight, i.e., the smaller the car, the greater the deceleration. This relationship is illustrated in Figure 2.1.

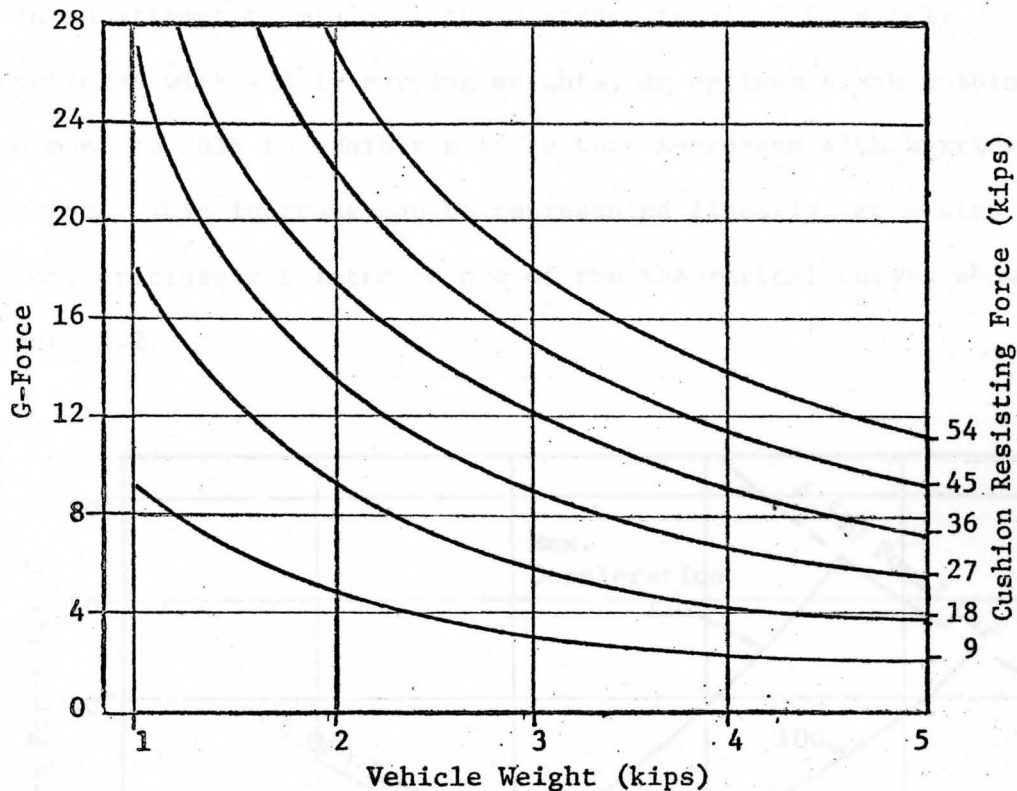


FIGURE 2.1 VEHICLE WEIGHT VS. DECELERATION

One approach to barrier design is to establish the barrier force necessary to stop a 2,000 pound car without producing excessive deceleration. The required crash cushion deformation length can then be determined from the following work-energy relationship:

$$U = \int F_x \cdot dx$$

where U is the work done by the crash cushion and is numerically equal to the kinetic energy of the impacting vehicle and where F_x is the crash cushion force acting on the vehicle through a small

crash cushion deformation d_x . For a cushion that deforms with a constant force F , the work, U , is the product of F and the total cushion deformation d , i.e., $U = F \cdot d$. Unfortunately, this design procedure produces installations too long and hence, impractical.

In an attempt to minimize the distance required to safely stop vehicles with widely varying weights, an optimum crash cushion design must be able to exhibit a force that increases with barrier deflection. This increase can be represented linearly, as a step function, or closely related to one of the theoretical curves shown in Figure 2.2.

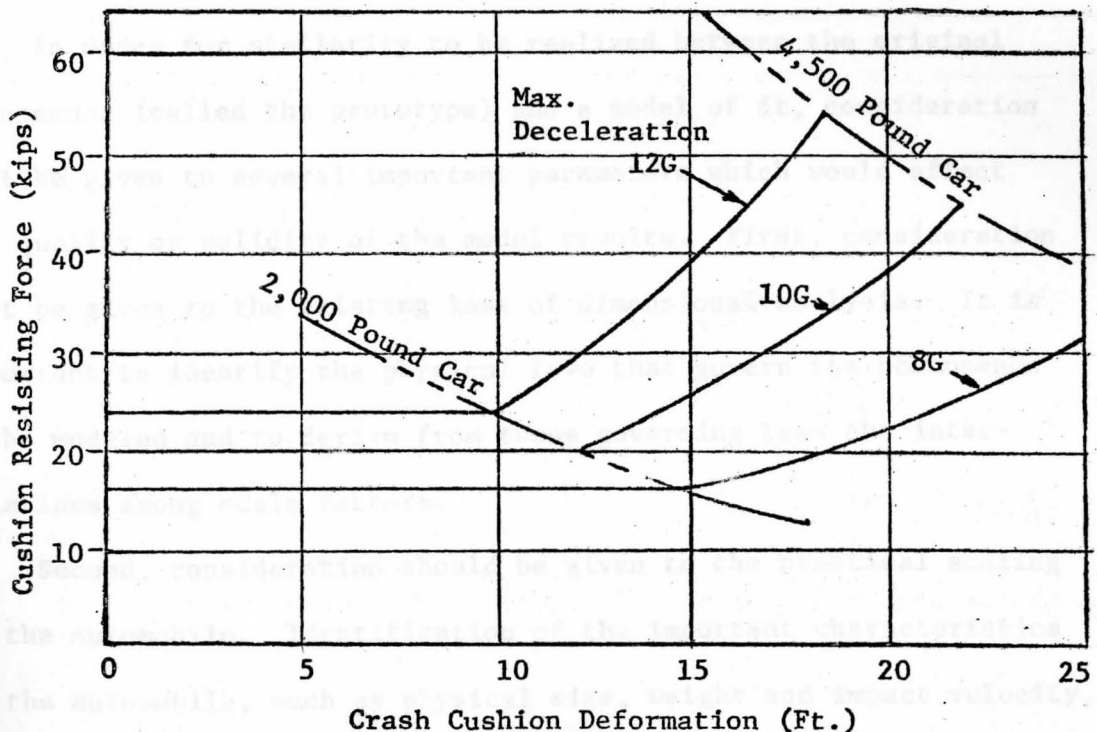


FIGURE 2.2
THEORETICAL BARRIER FORCE-DEFORMATION RELATIONSHIP
VEHICLE WEIGHTS: 2,000-4,500 POUNDS
VEHICLE VELOCITY: 60 MPH

A small car impacting such a barrier is decelerated to a stop by the initial part of the barrier, prior to excessive buildup of force. A heavier car is decelerated at a slower rate during the initial part of barrier deformation. Thereafter, deceleration increases to a more effective level with increased deformation.⁽¹⁰⁾ A more detailed analysis of such a crash cushion mechanism will be presented in a later chapter along with the results of the scale model tests.

2.2 Similitude

Now that the design criteria for crash cushions have been established, it will be necessary to formulate a set of scaling laws so that these criteria can be effectively applied to scale models.

In order for similarity to be realized between the original phenomenon (called the prototype) and a model of it, consideration must be given to several important parameters which would affect the quality or validity of the model results. First, consideration must be given to the existing laws of dimensional analysis. It is important to identify the physical laws that govern the phenomenon to be modeled and to derive from these governing laws the inter-relations among scale factors.

Second, consideration should be given to the practical scaling of the automobile. Identification of the important characteristics of the automobile, such as physical size, weight and impact velocity, and a determination as to whether these characteristics can be accurately and feasibly simulated.

Third, and most importantly, the accurate scaling of the light-weight concrete crash barriers must be studied. Emphasis must be

given to the following: a) The size effect of the lightweight concrete aggregate, i.e., if the size of the specimen is scaled down but the aggregate is not, will this affect the proper scaling of the energy absorption of the concrete? b) The modeling of the crash cushion shape, i.e., a configuration must be selected that will lend itself to proper scaling in terms of energy absorption (load-displacement relationship) and fracture pattern. These three aforementioned considerations must be discussed in detail.

For this study, it was considered desirable to have the model barrier made of the same material as the full-size prototype, i.e., low-density concrete. This meant that the density (ρ) and the modulus of elasticity (E) would be the same for model and prototype. Consideration was also given to the strain-rate sensitivity of the low-density concrete. It was shown previously⁽¹¹⁾ that any increase in impact velocity upon a confined lightweight concrete specimen would result in increased energy absorption by the specimen. It was assumed, therefore, that if the impact velocity of the scale model car was the same as that of the prototype, i.e., 60 mph, any effects due to velocity sensitivity could be ruled out.

Based upon these initial conditions, the Cauchy similitude laws⁽¹²⁾ were found to be applicable in this study. Table 2.1 lists the pertinent scale ratios derived from the Cauchy similitude laws. In this table, λ is the scale factor between model and prototype. The subscripts "p" and "m" identify prototype and model values respectively.

VARIABLE	SYMBOL	BASIC DIMENSIONS	SCALE RATIO
Length	L	L	$L_m = \lambda \cdot L_p$
Modulus of elasticity	E	M/LT ²	$E_m = E_p$
Concrete density	ρ	M/L ³	$\rho_m = \rho_p$
Area	A	L ²	$A_m = \lambda^2 \cdot A_p$
Volume	V	L ³	$V_m = \lambda^3 \cdot V_p$
Mass	M	M	$M_m = \lambda^3 \cdot M_p$
Velocity	V	L/T	$V_m = V_p$
Deceleration	a	L/T ²	$a_m = \lambda^{-1} \cdot a_p$
Force	F	ML/T ²	$F_m = \lambda^2 \cdot F_p$
Time	T	T	$T_m = \lambda \cdot T_p$
Stress	σ	M/LT ²	$\sigma_m = \sigma_p$
Strain	ϵ	-	$\epsilon_m = \epsilon_p$
Gravity	g	L/T ²	$g_m = \lambda^{-1} g_p$

TABLE 2.1
SCALE RATIOS CORRESPONDING TO THE
CAUCHY SIMILITUDE LAWS

2.3 Scale Model Vehicle Design

The cars used in the impact tests were modeled to a scale of 1:14 and were specifically weighted to simulate 2,000, 3,000, 4,000 and 4,500 lb. prototype vehicles. The scale factors for the model car

Cauchy's condition assumes that gravitational forces can be neglected, so that the similitude laws can be derived from the relation: $\frac{\text{inertia force}}{\text{elastic force}} = \text{constant}$. Therefore, if Cauchy similitude laws are used, gravitational forces are not correctly reproduced. From Table 2.1 it can be seen that gravity varies inversely with the size of the model. Thus, if gravitational forces are important they must be induced artificially in order to preserve the integrity of the scale modeling analysis. For this study, however, the effect of gravity can be considered negligible because the major forces on the model are much larger than the vehicle weight and are in a plane perpendicular to the gravitational forces.

Examination of Table 2.1 also reveals that the deceleration varies inversely with the size of the model and time varies proportionally with the size of the model. These two facts must be considered when analyzing the data from the high speed camera record of the model test crashes.

This brief presentation on similitude laws shows that a successful model of a vehicle-crash cushion response requires an exact duplication of the prototype crash cushion in reduced scale with the same material. The next two sections deal with the details of automobile and crash cushion modeling respectively.

2.3 Scale Model Vehicle Design

The cars used in the impact tests were modeled to a scale of 1:14 and were specifically weighted to simulate 2,000, 3,000, 4,000 and 4,500 lb. prototype vehicles. The scale factors for the model car

mass, length, width, and velocity were respectively λ^3 , λ , λ , and 1, or where λ equals the scale factor of 1:14.

The linear dimensions, the weight and the velocity of the model vehicle and the prototype were given primary consideration. Other factors, such as tire friction, tire spring constant, and ground pressure were not considered significant because the tests were confined to a straight head-on impact where it could be assumed that these factors would play a negligible role.

Since automobiles come in different weights, shapes and sizes, it was necessary to search out significant data with which to form composite cars for each of the available classes. Since an impact attenuator's performance is dictated by the weight and speed of the impacting automobile, it was decided to have classes designed by vehicular weight since the impact speed would be held constant for all the tests. From previous studies,⁽¹³⁾ it was found that approximately 85% of all automobiles weigh between 2,000 and 4,500 lbs. Further studies⁽¹⁴⁾ have revealed that intermediate classes can be established at weights of 3,000 and 4,000 lbs. since the distribution of cars between 2,000 and 4,500 lbs. is such that large concentrations of vehicles exist at or near these points (see Figure 2.3).

With the weight classes so determined, it then became necessary to compile pertinent data, e.g., length and height, in order to formulate average vehicle parameters for the different weight classes. This data was collected by visiting the various new car dealers in the surrounding area. In order to obtain a sufficient sampling, the following dealers were visited: Ford, Volkswagen, AMC, and General

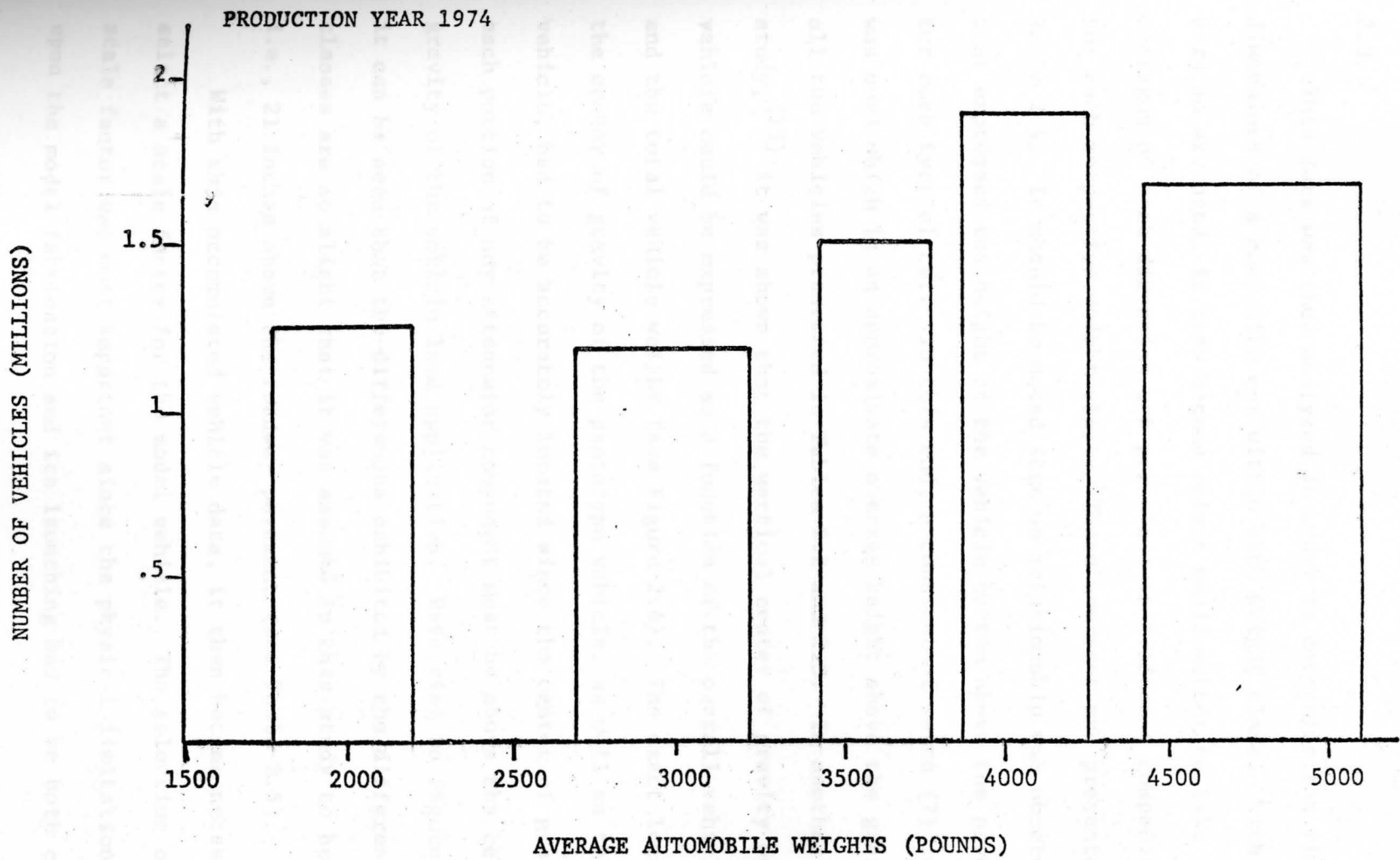


FIGURE 2.3

Motors. The resulting accumulated data is shown in Tables 2.2 and 2.3.

This data was then analyzed in order to determine the final dimensions of a composite car within each weight class. With the cars so arranged, it then became only a small matter to take the averages of each dimension set per class to produce a composite car for each respective weight class. These averages are presented in Table 2.4. It should be noted that no relationship was observed that expressed the height of the vehicle bottom above the pavement for each type of car. To this end, a constant of seven (7) inches was used which is an approximate average height above the ground for all the vehicles presented in Tables 2.2 and 2.3. In another previous study,⁽¹⁵⁾ it was shown that the vertical center of gravity of each vehicle could be expressed as a function of the overall vehicle height and the total vehicle weight (see Figure 2.4). The exact location of the center of gravity of the prototype vehicle, as well as the model vehicle, had to be accurately located since the center of gravity of each portion of any attenuator component must be above the center of gravity of the vehicle load application. Referring to Figure 2.4, it can be seen that the differences exhibited by the different weight classes are so slight that it was assumed in this study to be constant, i.e., 21 inches above the roadway pavement (see Table 2.5).

With this accumulated vehicle data, it then became necessary to select a scale factor for the model vehicle. The selection of a basic scale factor was most important since the physical limitations imposed upon the model fabrication and its launching had to be both considered

MODEL	LENGTH (in.)	WIDTH (in.)	WHEEL- BASE (in.)	HT. (in.)	WT. (lb.)	FRONT TREAD (in.)	REAR TREAD (in.)	GROUND CLEARANCE (in.)
<u>FORD</u>								
Maverick	187.0	70.5	103.0	52.9	2929	56.5	56.5	7.2
LTD	223.9	79.5	121.0	53.7	4446	64.0	64.0	7.6
Granada	197.7	71.2	109.9	53.3	3356	56.5	56.5	7.2
Pinto	169.0	69.4	94.5	50.6	2575	54.0	54.0	6.9
Torino	214.4	79.3	114.0	52.6	4178	63.4	63.5	7.1
Mustang II	175.0	70.2	96.2	50.0	2784	55.0	55.0	7.0
<u>GM</u>								
Impala	222.9	79.5	121.5	54.4	4301	64.1	64.0	7.2
Chevelle	207.5	74.4	114.0	53.1	4000	61.5	60.7	7.2
Monte Carlo	212.7	77.6	116.0	52.7	4000	61.9	60.7	7.3
Vega	175.4	65.4	97.0	51.8	2800	54.8	53.6	6.2
Camaro	195.4	74.4	108.0	49.1	3650	61.3	60.0	6.0

TABLE 2.2
TYPICAL VEHICLE DIMENSIONS (1976 MODELS)

MODEL	LENGTH (in.)	WIDTH (in.)	WHEEL- BASE (in.)	HT. (in.)	WT. (lb.)	FRONT TREAD (in.)	REAR TREAD (in.)	GROUND CLEARANCE (in.)
<u>AMC</u>								
Pacer	170.0	77.0	100.0	52.7	3180	61.2	60.2	6.1
Gremlin	169.4	70.6	96.0	52.3	2831	57.5	57.1	5.7
Hornet	186.0	71.0	108.0	52.2	2986	57.5	57.1	6.2
Matador	216.0	75.7	118.0	54.7	3670	59.8	60.0	6.4
<u>VW</u>								
Scirocco	155.7	63.9	94.5	51.6	1950	50.0	50.0	6.6
Dasher	172.4	63.0	97.2	53.5	2125	50.0	50.0	6.5
Rabbit	155.3	63.4	94.5	55.5	1850	50.0	50.0	6.5
Beetle	163.4	61.0	94.5	59.1	1935	49.0	49.0	5.9

TABLE 2.2 (continued)

MODEL		VEHICLE WEIGHT
GROUP 1 2000 LB.	RABBIT	1850 lbs.
	BETLE	1935
	SCIROCCO	1950
	DASHER	2125
GROUP 2 3000 LB.	PINTO	2575
	MUSTANG II	2704
	VEGA	2800
	GREMLIN	2831
	MAVERICK	2929
	HORNET	2986
	PACER	3180
GRANADA	3356	
GROUP 3 4000 LB.	CAMARO	3650
	MATADOR	3670
	MONTE CARLO	4000
	CHEVELLE	4000
	TORINO	4178
	IMPALA	4301
	LTD	4446

TABLE 2.3
GROUPINGS FOR VEHICLE PARAMETER AVERAGING

NOTE: The composite vehicle dimensions for the 4500 lb. car are approximately linear extensions of the vehicle data for the three known classes.

WEIGHT	LENGTH (in.)	WIDTH (in.)	HEIGHT (in.)	WHEEL- BASE (in.)	FRONT TREAD (in.)	REAR TREAD (in.)	HEIGHT OF FRONT AREA (in.)	FRONTAL AREA (in.)
2000 lbs.	161.7	62.8	54.9	95.2	50.0	50.0	22.0	1381.6
3000 lbs.	178.7	70.7	51.9	100.6	56.6	56.25	23.0	1626.1
4000 lbs.	214.7	77.5	52.9	116.1	62.3	61.8	24.0	1860.0
4500 lbs.	227.0	83.5	53.5	122.0	67.0	67.0	26.0	2171.0

TABLE 2.4
COMPOSITE CAR DIMENSIONS (PROTOTYPE)

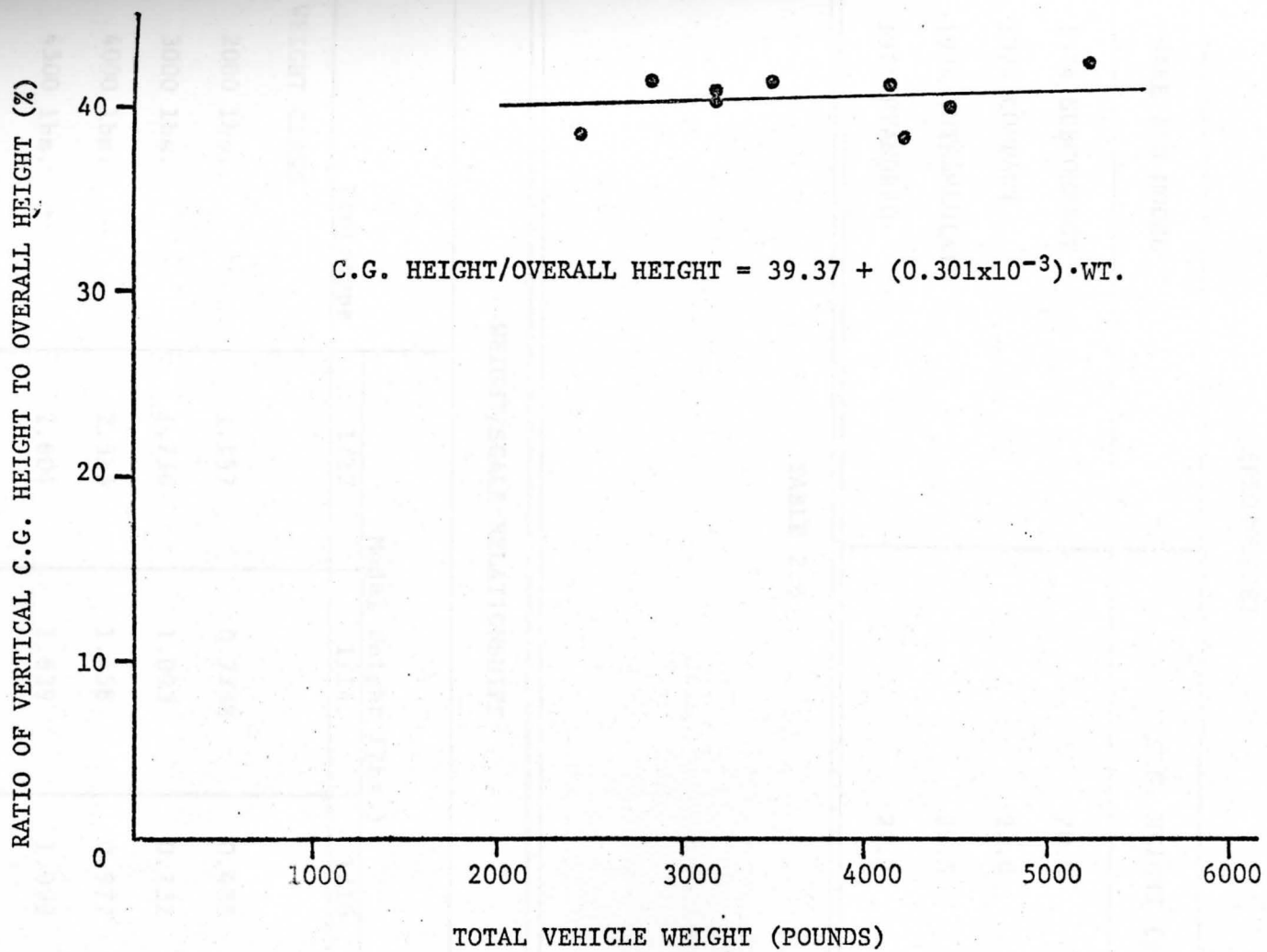


FIGURE 2.4
 TOTAL VEHICLE C.G. HEIGHT AS A FUNCTION OF TOTAL WEIGHT

COMPOSITE CENTER OF GRAVITY HEIGHT (PROTOTYPE)	
MAKE AND MODEL	C.G. HEIGHT (in.)
1974 SUBCOMPACT	20.0
1974 COMPACT	22.0
1974 INTERMEDIATE	20.5
1974 STANDARD	21.7

TABLE 2.5

WEIGHT/SCALE RELATIONSHIPS			
Prototype	Model Weight (lbs.)		
	1/12	1/14	1/16
WEIGHT CLASS			
2000 lbs.	1.157	0.7288	0.488
3000 lbs.	1.736	1.093	0.732
4000 lbs.	2.315	1.458	0.977
4500 lbs.	2.604	1.639	1.099

TABLE 2.6

in its selection. For the actual scale factor chosen, several other important vehicle specifications were also considered with respect to the ultimate impact testing. These specifications summarize as follows:

- 1) The vehicle must be as rigid as possible.
- 2) The mass must be correct.
- 3) The vehicle center of gravity must be properly modeled.
- 4) The model materials must be as lightweight and strong as possible.
- 5) The model vehicle must be geometrically correct.
- 6) The model must be of sufficient size and weight that enables it to be modeled accurately.

With the aforementioned specifications in mind, it became clear that a weight-size relationship controlled the modeling problem. The problem degenerated into one of selecting a scale which would permit the construction of small models and yet would have a sufficient amount of weight with which to build scale models of good quality. Table 2.6 shows several scale choices along with the respective model weight. In this case, a 1:14 scale produced models which were easy to handle and fabricate with respect to both size and weight. The basic form of the test models was limited by the weight and geometric considerations. Limited to a specified wheel-base, the design process proceeded to place the available building materials in a form which would adhere to the specifications. This was accomplished by having the vehicle assume a basic form of inter-connected blocks recalling that the important model parameters are the location of the vertical center of gravity and the mass requirements as well as ease of con-

struction. This basic form is illustrated in Figure 2.5. Since the wooden blocks were to be the predominate material, their selection formed the basis from which the other model materials would be selected. In other words, the shear volume of the end blocks had such a domineering effect on the total model weight that the other materials were required to be of sufficiently low-density so that the total weight of all the materials would be less than or equal to the required weight of the model car. After some investigation, redwood was selected for the end block material. Redwood possessed lowest density and yet met all of the other required criteria, i.e., low density, availability, high strength, and high penetration resistance.

Crash plates were added to the front of the model vehicles to eliminate any penetration that might occur during impact. Aluminum was the lightest and strongest available material and thus, was used for both the crash plates and when necessary to adjust the vertical center of gravity. The connecting rods used to space the wooden end blocks presented another significant design problem. Not only were they required to fasten together the wooden end blocks and thus maintain the required wheelbase, but they were also required to transfer impact impulses across their lengths from the front to the end blocks. Since the front and rear blocks were held at a constant center of gravity height, the connecting rods were placed so that their center of gravity had the same vertical position as the end blocks. A connecting material was required, therefore, which was not only lightweight, but also minimized any axial displacements under the impact loading. Plexiglas was eventually selected due to both its lightweight

and strength qualities. The rolling wheels of the model vehicles were not crucial with respect to the mass calculations, but were important from their tire-road interface frictional effect. With this in mind, the tire and wheel components were selected in an attempt to maintain size and scale, but concentrating more so on correctly modeling the tire-road interface friction. The wheels and tires finally selected were a common type used for "slot cars" and were attached directly to steel axles. This selection of tires was felt to accurately model the rolling resistance experienced by the prototype vehicles.

When a full-size automobile is in forward motion and impacts a barrier or an obstacle, any rebound motion of the vehicle is restricted by the resistance of the transmission to undergo a reverse motion when a forward gear is engaged at the instant of impact. To accomplish this phenomenon in the models, it became necessary to construct a brake to prevent the reverse rolling of the wheels after the collision with the model attenuator. In the models this was accomplished by having a 1/16 spring steel wire connected between the two rear wheels. This is outlined in detail in Figure 2.7.

Figure 2.6 and Table 2.7 jointly show all the significant dimensions in detail for all the weight classifications selected. These dimensions and parameters accurately model the composite vehicles originally selected. Trim, targets, painting, etc., were added later to increase the aesthetic effect of the vehicles. The photographs shown in Figures 2.8 and 2.9 show the completed models prior to testing.

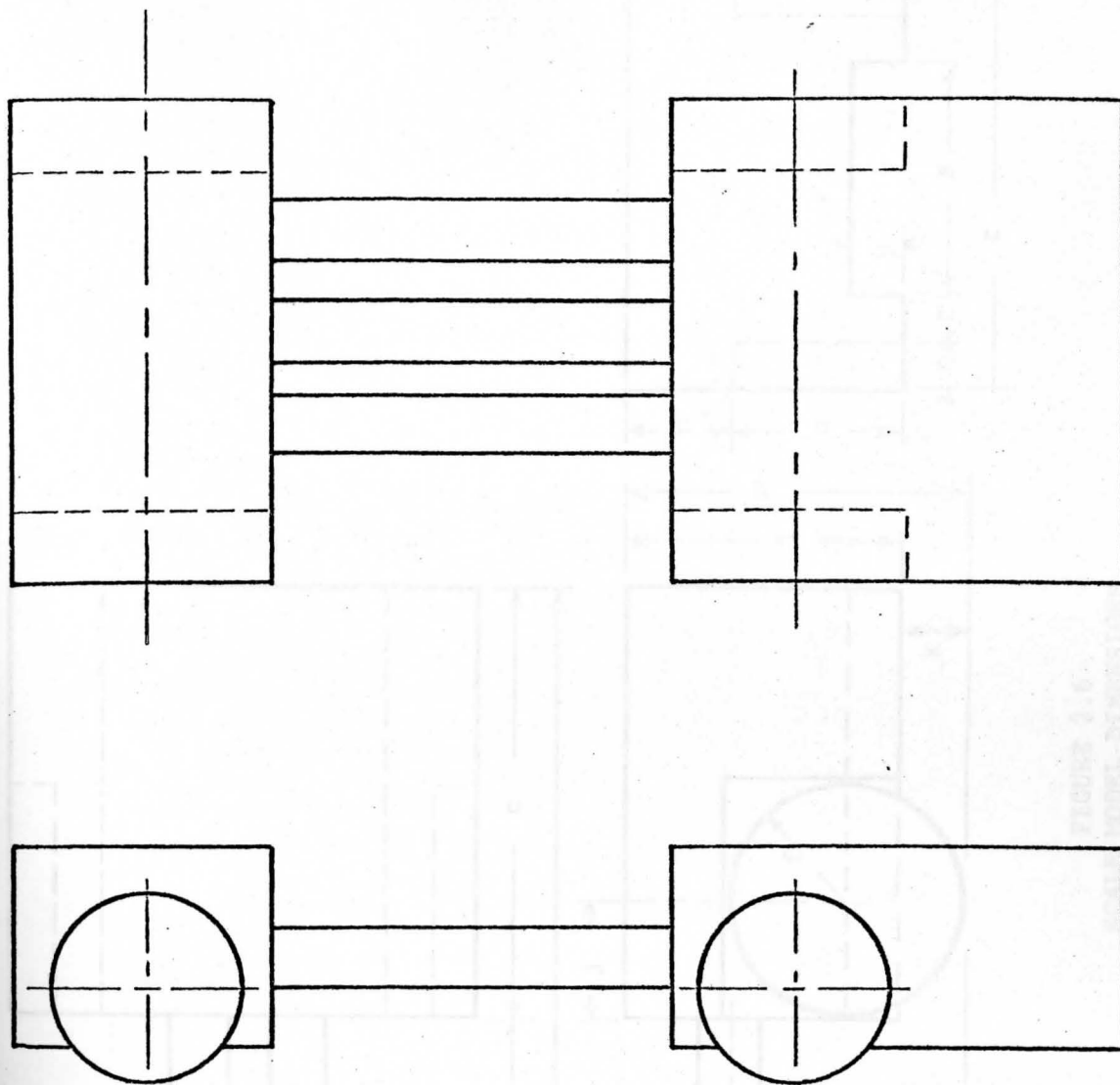


FIGURE 2.5
BASIC MODEL VEHICLE FORM

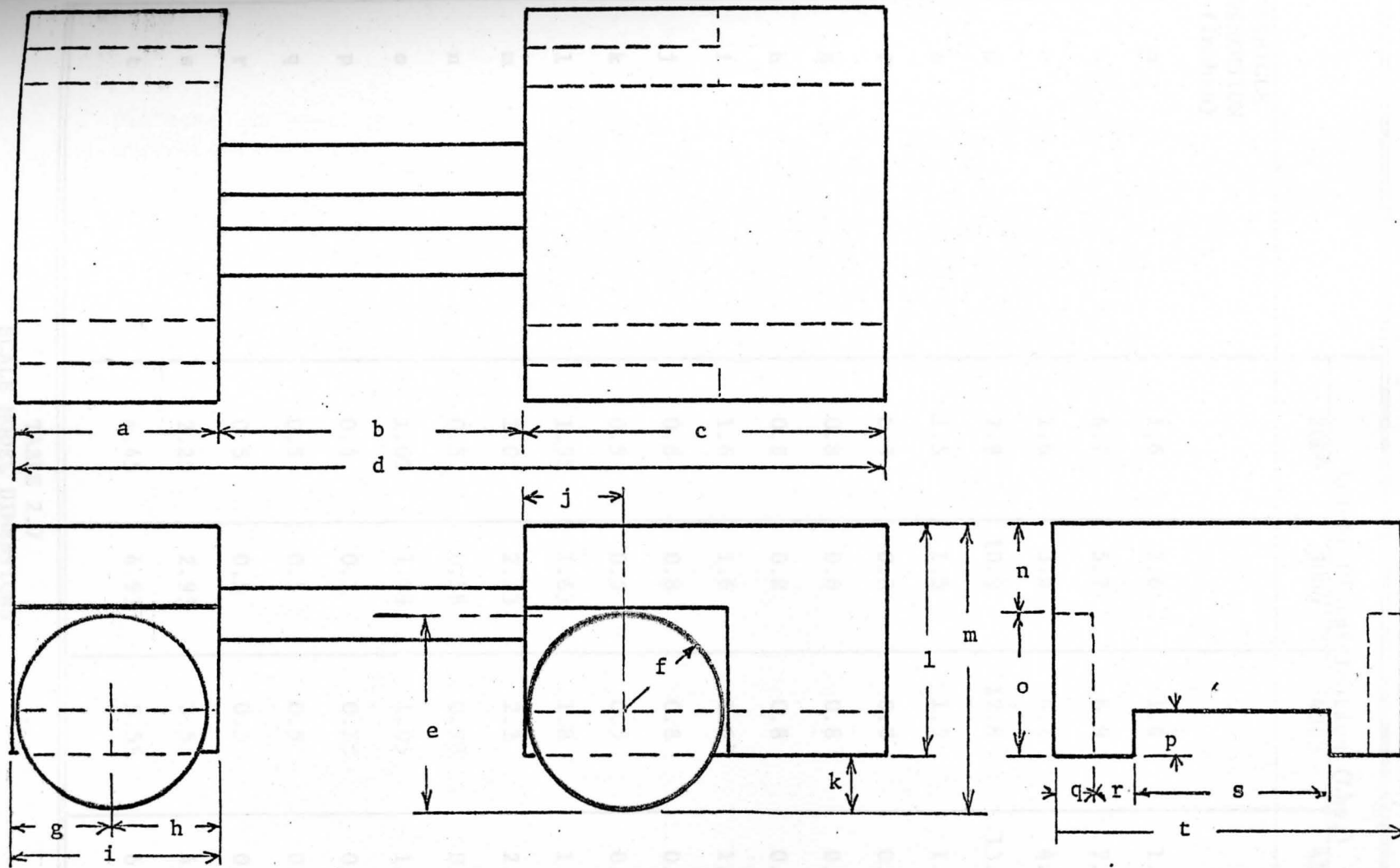


FIGURE 2.6
SCALE MODEL DIMENSIONS

VEHICLE DIMENSION (Inches)	Weight Classification (Lbs.)			
	2000	3000	4000	4500
a	1.6	1.6	1.6	1.6
b	4.7	5.7	6.9	7.3
c	1.6	3.5	4.1	4.5
d	7.9	10.9	12.8	13.5
e	1.5	1.5	1.5	1.5
f	0.8	0.8	0.8	0.8
g	0.8	0.8	0.8	0.8
h	0.8	0.8	0.8	0.8
i	1.6	1.6	1.6	1.6
j	0.8	0.8	0.8	0.8
k	0.5	0.5	0.5	0.5
l	1.55	1.63	1.8	1.9
m	2.05	2.13	2.3	2.4
n	0.5	0.58	0.75	0.85
o	1.05	1.05	1.05	1.05
p	0.4	0.3	0.15	0.4
q	0.5	0.5	0.5	0.5
r	0.5	0.5	0.5	0.5
s	2.25	2.93	3.55	4.00
t	4.45	4.93	5.55	6.00

TABLE 2.7
SCALE MODEL DIMENSIONS

The steel is bent in such a way that the brake wire just makes contact while the car is in forward motion, and bites into the tire upon reverse motion.

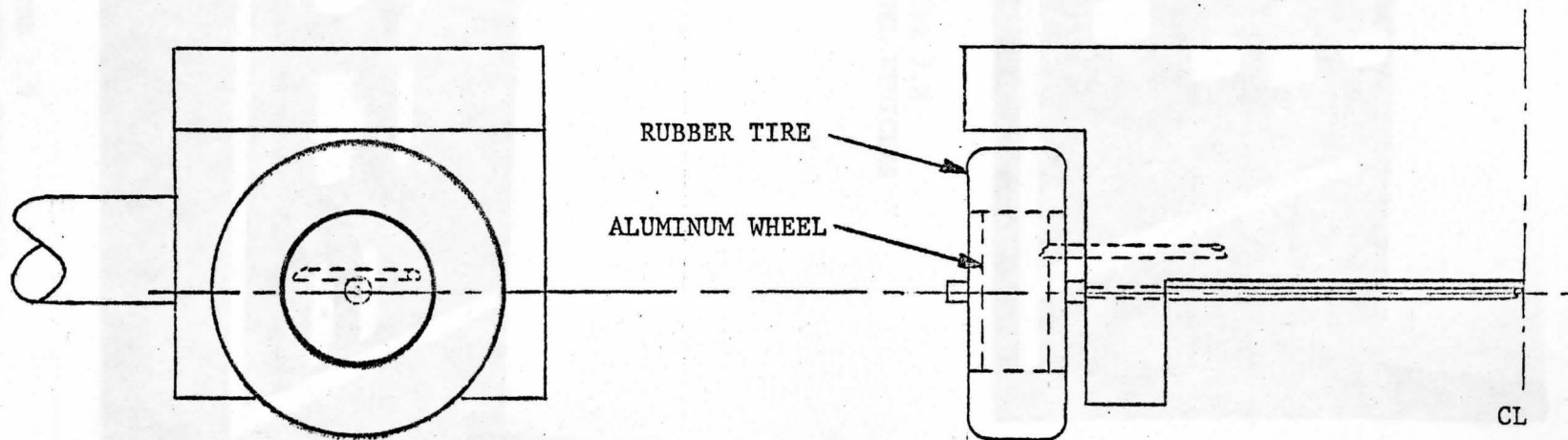
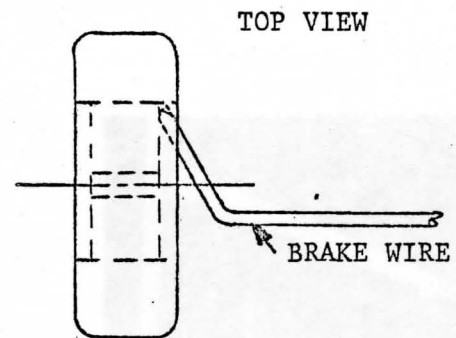


FIGURE 2.7
WHEEL REVERSE BRAKE

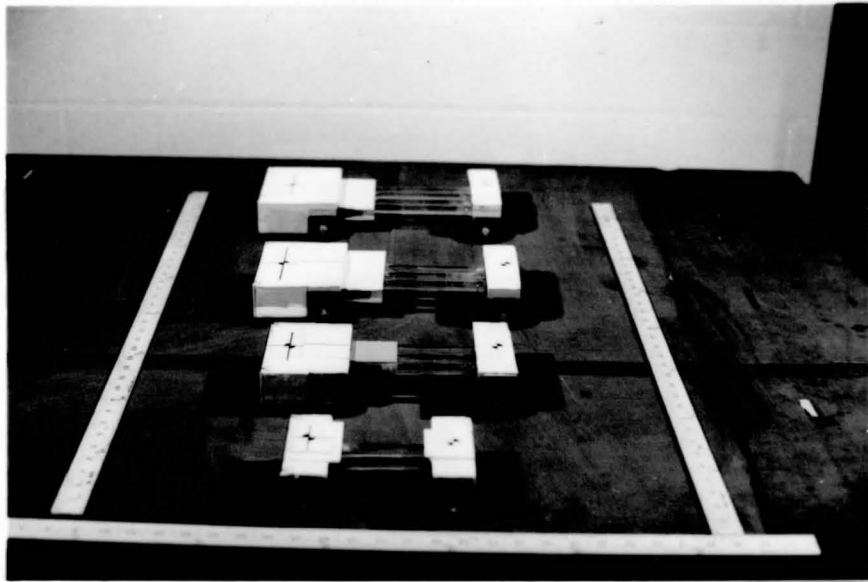


FIGURE 2.8
SCALE MODEL VEHICLES

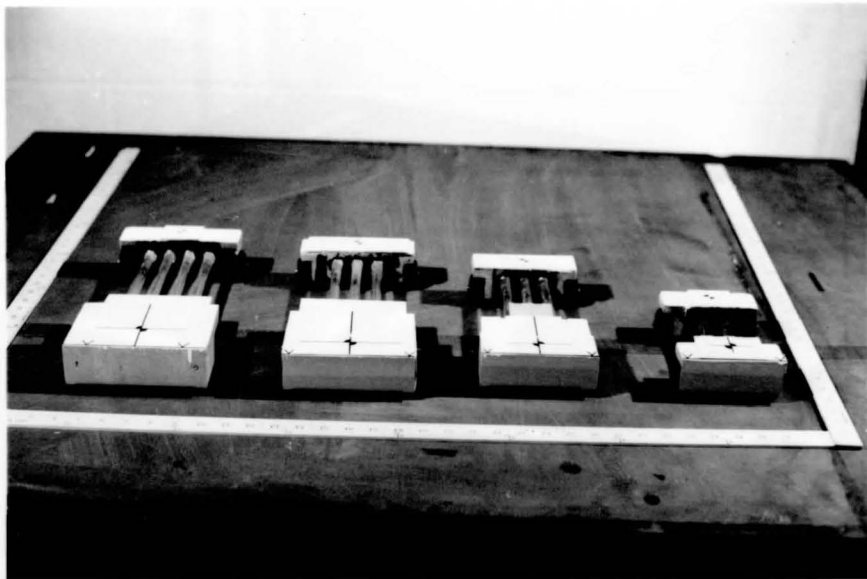


FIGURE 2.9
FROM LEFT TO RIGHT: SCALE MODEL
4,500, 4,000, 3,000 AND 2,000 POUND VEHICLES

2.4 Scaling Effects of Lightweight Aggregate

The last and most important preliminary study conducted dealt with the effects of scaling lightweight concrete. As mentioned previously, this study was broken down into two phases. The first phase investigated the effects of the lightweight aggregate in the accurate scaling of this type of concrete. Previous studies indicate that crushing tests performed on normal concrete show a general trend that the smaller a concrete test cube or cylinder the higher its failure stress. If this same phenomenon were to exist in lightweight concrete, then no reliance could be placed on the small scale tests using the same size aggregate as the prototype tests.

The purpose of this phase of study was to determine at what scale a linear relationship would no longer exist in projecting the energy absorption of low-density concrete.

The concrete chosen for this study was Dycon* IV. This concrete contains a polystyrene aggregate consisting of 1/16, 1/8, and 3/8 inch diameter spheres (see Figure 2.10). This concrete was chosen because it is the most critical of all of the Dycon types in determination of scale relationships, i.e., Dycon I, II, and III contain polystyrene aggregate of uniform size, namely 1/16 inch in diameter.

Static tests of Dycon IV cubes ranging in size from 1 inch on a side to 30 inches on a side were performed using the 120,000 pound and 600,000 pound Universal Testing Machines. Specimens ranging in size up to 12 inches on a side were crushed to 50% of their original height. Values of energy for these larger specimens were obtained

*Dycon is a registered trademark of Koppers Company, Inc.

using linear extrapolation.

Values of absorbed energy in in.-lb. obtained from these static tests were then plotted against the volume of the specimen (in.³). The sheer physical size of a graph needed to plot the wide range of values obtained made it impractical to plot the data points. This problem made the use of the high speed computer and some basic statistical relationships valuable tools in the determination of the solution to the problem. From the statistical evaluation of the data, a size could then be determined at which a linear scale relationship no longer exists.

Since this project deals with the behavior of the Dycon IV under dynamic loading conditions, i.e., a model car impacting a model impact attenuator, it was initially decided that the specimens should be crushed dynamically by fabricating an impacting machine. The Dycon IV, however, absorbs a tremendous amount of energy under dynamic conditions and it was decided that a number of machines would have to be built to accommodate the range of specimens to be tested. Since the time, facilities, and raw materials were not available to produce such machines, the possibility of static testing was investigated.

Static testing was chosen for a number of reasons. First, static testing machines were readily available. Secondly, the vast majority of the specimens could be tested on machines that plot load vs. deflection as the test takes place. Thirdly, it was decided that any variations in scale shown by the dynamic studies would appear in the static studies as long as all of the specimens were

tested under as identical conditions as possible. For those reasons, static testing was chosen as the route to follow in the energy determinations.

The following sizes of specimens were tested. (Note that all specimens were cubes and thus only one dimension is given): 1 in., 1½ in., 2 in., 3 in., 4 in., 5 in., 6 in., 7 in., 8 in., 12 in., 16 in., 20 in., 24 in., and 30 in. (see Figure 2.11). Specimens smaller than 7 in. were cut from 7 in. cast specimens. Larger specimens were cast to size. One in. and 1½ in. specimens were tested on the machine shown in Figure 2.12. Load and deflection were tabulated and then plotted. Specimens ranging in size from 2 in. to 8 in. were tested on a 120,000 pound Universal Testing Machine. Larger specimens were tested on a 600,000 pound Universal Testing Machine, for which a special rigid loading head had to be fabricated. Graphs for load vs. deflection were obtained from the machines' strain follower adaptor. These graphs automatically provided a vertical axis of load in pounds and a horizontal axis of deflection in inches. The area under this curve to a deflection of 50% of the specimens original vertical height was taken to represent the energy absorbed.

These areas were determined by the use of a K&E compensating polar planimeter. Values of area were tabulated for a number of each size of specimen tested, then from these an average area was determined for each size. These values are tabulated in Table 2.8.

The range of data determined from testing specimen volumes from 1 in.³ to 27,000 in.³ along with energy absorptions of 42.11 in.-lb.

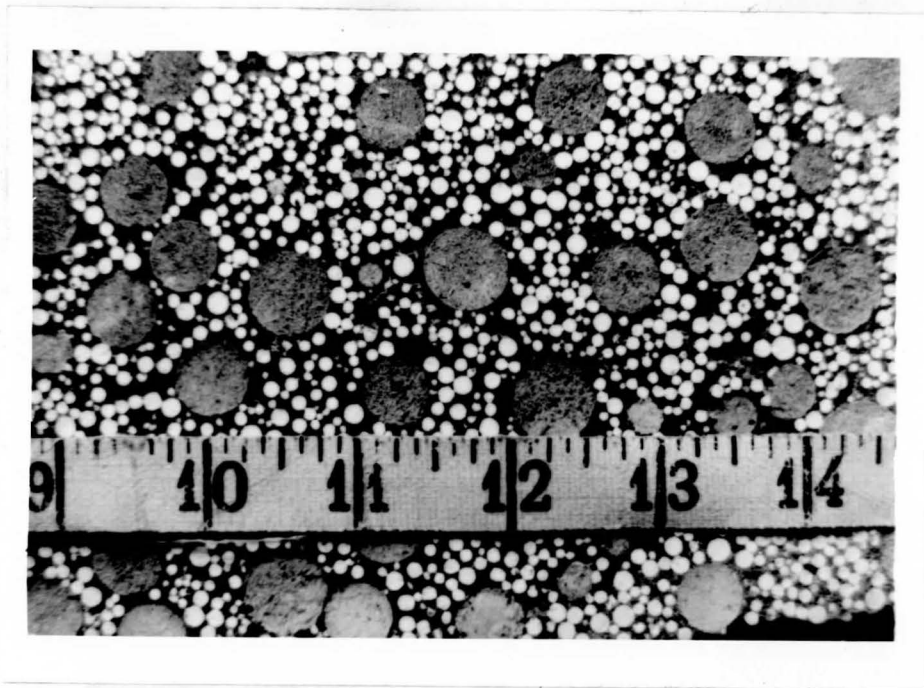


FIGURE 2.10
DYCON IV CONCRETE MATRIX



FIGURE 2.11
1 INCH TO 30 INCH DYCON IV CUBES



FIGURE 2.12
APPARATUS FOR THE STATIC COMPRESSION
TESTING OF 1 IN. AND 1.5 IN.
DYCON IV CUBES

SIZE OF CUBE (in.)	VOL. OF CUBE (in. ³)	NO. OF SPECIMENS TESTED	E_s^* (in.-lb.)	STD. DEV.	AVG. MAXIMUM INITIAL LOAD (lb.)	STD. DEV.
1.0	1.000	8	38.42	7.22	89.88	15.38
1.5	3.375	8	131.13	12.45	191.25	29.49
2.0	8.000	8	377.78	46.12	397.13	78.85
3.0	27.000	8	1502.80	323.22	1157.25	308.96
4.0	64.000	5	3194.5	432.51	1820.00	313.75
5.0	125.000	5	5593.75	578.14	2412.8	192.33
6.0	216.000	5	9787.88	1218.11	3773.8	556.63
7.0	343.000	5	12318.68	1610.51	4263.8	498.54
8.0	512.000	5	22405.27	3130.05	6328.20	1180.93
12.0	1728.000	5	83415.38	14076.08	15904.00	3468.52
16.0	4096.000	4	223057.43	19534.86	29187.50	5255.49
20.0	8000.000	2	440150.38	35597.16	47500.00	3535.53
24.0	13824.000	3	754047.00	67795.70	69700.00	5741.95
30.0	27000.000	3	1231740.10	143979.12	96166.67	22250.47

TABLE 2.8
AVERAGE VALUES FOR ENERGY ABSORPTION

*Average energy consumed in the static crush of the specimen to 50% deformation.

to 1,231,740 in.-lb. respectively, made the drawing of a single graph with any accuracy impossible. The use of the IBM 370 computer and the Stat-Basic Package available through the Youngstown State University Computer Center expedited the determination of the linearity of the data.

Absorbed energy to 50% deformation in in.-lb. vs. specimen volume in in.³ was plotted. If a linear relationship existed for this parameter, then a linear scale relationship would also exist for the model and the full size prototype. From Table 2.8 fourteen data points, i.e., volume vs. energy absorbed, were available. With the origin, this gave a total of fifteen points with which to work.

The data points were arranged in sets of three: where set 1 = 0 in³, 1 in³, 3.375 in³; set 2 = 1 in³, 3.375 in³, 8 in³; set 3 = 3.375 in³, 8 in³, 64 in³, and so on until thirteen data sets were arranged. The least squares method of fitting a line was used in the Stat-Basic Package to determine the equation of the line for each set of data. The slope, the y-intercept, and the correlation coefficient* for each of the lines formed by the three data points were computed. If values of slope and y-intercept were similar in magnitude for each segment, i.e., three point line, and the correlation coefficients for each sequential line segment were near one, then there was a good possibility of working a straight line through the entire set of data. If the values of slope and y-intercept were not similar in magnitude, then the data were either not at all linear, or it represented two or more straight lines, i.e., the entire set of data did not fit one

*See Appendix A for mathematical explanation of these terms.

single straight line. Proceeding in this manner, the statistical results obtained are presented in Table 2.9.

A study of slope and y-intercept for absorbed energy vs. volume (Table 2.9) shows a close similarity between the various values of slope and y-intercept. The correlation coefficients are also quite close to 1.0 for the incremental lines.

Armed with the fact that the absorbed energy vs. volume is a linear function for Dycon IV, it was decided to look at the change in slope between sequential three point lines (Table 2.10). Very small percentage differences between sequential three point line segments would indicate that all of the data fits a single straight line. Any large change of slope between sequential segments would indicate a possible break in a single linear relation of the data. In Table 2.10 it can be seen that between data sets 8 and 9 there is a 52.91% change in slope in the case of absorbed energy vs. volume. Data set 8 represents volumes of 216 in.³, 343 in.³, and 512 in.³, and data set 9 represents volumes of 343 in.³, 512 in.³, and 1728 in.³, which would indicate a change is present between specimen volumes 343 in.³ and 512 in.³. The data were divided between these two points and two lines were placed through the two separate sets of data using a least squares fit. This least squares fit produced the following linear formulas:

Points: Origin - 216 in

$$y=45.06x+78.27$$

y=energy (in.-lb.)

x=volume (in.³)

$$45.06 \frac{\text{in.-lb.}}{\text{in.}^3} = \text{slope}$$

78.27 in.-lb. = y-intercept

r=correlation coefficient=0.999193216

Points: 343 in.³ - 27,000 in.³ $y=46.66x+25,626.56$
 $y=\text{energy (in.-lb.)}$
 $x=\text{volume (in.³)}$
 $46.66 \frac{\text{in.-lb.}}{\text{in.³}} = \text{slope}$
 $25,626.56 \text{ in.-lb.} = \text{y-intercept}$
 $r=\text{correlation coefficient}=0.994508956$

The change in slope between these two lines is 3.43% which is not a substantial change. The large change in magnitude of y-intercept values indicates, however, that some change in the linearity or an error exists in the last points of the graph.

Values for points 4,096 in.³ - 27,000 in.³ all contained extrapolated values. These values were obtained by linear extrapolation to 50% deflection. The actual test values acquired for the deflections were as low as 31.50% due to testing machine limitations. During the test, the applied load increased substantially as the deflection increased. This was characteristic for all the range of specimens tested. For this reason the last points of the graph were eliminated and the first 11 points (origin - 1,728 in.³) were used for a least squares fit. This process was repeated for the first 12 points (origin - 4,096 in.³) and the first 13 points (origin - 8,000 in.³). In the case of the 4,096 in.³ and 8,000 in.³ specimens, only one value for each size was obtained by extrapolation. Least squares fits values of absorbed energy were then forecast for the larger specimens and these are shown in Table 2.11. The correlation coefficient in Table 2.11 for the first 12 points (origin - 8,000 in.³) is 1.000. This would indicate that the data fits a straight line perfectly. By hand calculations this correlation coefficient was found to be 0.999640061. This value is sufficiently close to unity and thus, it can be

TABLE 2.9
CASE: Energy vs. Volume

SET NO.	a	b	r
1	39.17	51.95	0.999743805
2	47.69	-14.53	0.997541243
3	48.54	-28.02	0.997898460
4	51.56	-52.50	0.999620353
5	48.34	107.79	0.996821258
6	41.50	442.06	0.999162273
7	43.59	307.61	0.999099883
8	31.77	2102.82	0.979434169
9	48.58	-1906.85	0.969394492
10	50.30	-3329.61	0.999354844
11	56.04	-8244.67	0.999004101
12	56.75	-12633.76	0.999875775
13	54.53	1276.97	0.999963089
14	40.74	145596.62	0.994914647

$y = ax + b$
 $y = \text{energy (in.-lb.)}$
 $x = \text{volume (in.}^3\text{)}$
 $b = \text{y-intercept (in.-lb.)}$
 $a = \text{slope } \left(\frac{\text{in.-lb.}}{\text{in.}^3} \right)$
 $r = \text{correlation coefficient}$

SET NO.	Energy vs. Volume	
	Change in Slope	% Difference
1-2	-8.52	21.75
2-3	-0.85	1.78
3-4	-3.02	6.22
4-5	3.22	-6.24
5-6	6.84	-14.15
6-7	-2.09	5.04
7-8	11.82	-27.12
8-9	-16.81	52.91
9-10	-1.72	3.54
10-11	-5.74	11.41
11-12	-0.71	1.27
12-13	2.22	-3.91
13-14	13.79	-25.29

TABLE 2.10
CHANGE IN SLOPE

Size	No.	Actual % Crushed	Area @ Actual % Crushed	in.-lb. Extrapolated Area	in.-lb. Forecasted Area
13,824 in. ³	1	40.29	584,096.27	724,910.05	757,616.00
	2	47.08	782,925.53	831,540.32	
	3	44.58	629,148.93	705,690.64	
27,000 in. ³	1	35.15	763,351.06	1,085,815.70	1,481,451.10
	2	36.83	910,308.50	1,235,712.90	
	3	40.59	1,115,265.96	1,373,691.71	

Points 1-14 (origin-8,000 in.³) $y=54.94x-1,818.13$
 y =energy (in.-lb.)
 x =volume (in.³)
 $54.94 \frac{\text{in.-lb.}}{\text{in.}^3} = \text{slope}$
 $-1,818.13 \text{ in.-lb.} = y\text{-intercept}$
 $r=\text{correlation coefficient}=1.000$

TABLE 2.11
 FORCASTED VS. EXTRAPOLATED ENERGY ABSORPTION

concluded that the data for specimen sizes up through the including 20 in. on a side are linear. Energy values obtained from the larger specimens tested were in error due to the inability of the 600,000 pound Universal Testing Machine to crush the large specimens to 50% of their original height. Forecasted values for the 13824 in.³ and 27000 in.³ specimens were 757,616 in.-lb. and 1,481,451 in.-lb. respectively as compared to extrapolated values of 754,047 in.-lb. and 1,231,740 in.-lb. respectively.

From this phase of the study it can be concluded that for the range of size of specimens tested, a minimum size does not exist at which a model of a full size specimen no longer exhibits the properties of its full size counterpart with respect to energy absorption.

It would, however, be beneficial to perform a series of dynamic tests on a range of sizes of small specimens to compare the linearity of dynamic energy absorbed to the linearity of static energy absorbed. Such tests were not within the scope of this study but would be recommended if further investigations into the energy absorption characteristics of Dycon IV were to be performed.

2.5 Scaling Effects of the Crash Cushion Shape

The last phase of the preliminary study dealt with the selection of the crash cushion configuration to include a study of the scaling of this configuration and its fracture pattern upon collision.

The Texas Transportation Institute⁽¹⁶⁾ has conducted a number of full scale crash tests on cushions made with lightweight vermiculite concrete. The basic shape of these cushions can be seen in Figure

2.13. Since there is a considerable amount of data available on these tests, it was decided to adopt the same basic shape for use in this scale model study. It should be mentioned that no attempt will be made to correlate the results of this scale model study with the Texas tests. However, since it has been shown that this particular shape does have merit, it seemed like the logical place to start.

A closer examination of Figure 2.13 shows that the crash cushions are constructed by the longitudinal stacking of a series of precast concrete modules. The individual modules were made of light-weight vermiculite concrete, are rectangular in shape (plan view), and have either two or three large cylindrical voids. These voids were obtained by placing cardboard sonotubes into a rectangular form and backfilling the form with concrete. These cylindrical voids presented problems when attempts were made to fabricate a 1/14 scale model module, to say nothing of the fabrication problems and expenses encountered during the Texas tests with circular voids and cardboard tubes. It was decided, therefore, to search for an alternate module shape that would be both inexpensive and easier to mold in both scale and prototype. Diamond, hexagon and rectangular shaped voids were studied and ultimately the rectangular shape was selected. This shape offered easier fabrication and better control of wall thicknesses. The basic crash cushion with rectangular shaped voids is shown in Figure 2.14. Numerous preliminary designs which utilized the load-deflection relationships of the other void shapes (both model and prototype) were made and further confirmed the rectangular void selection.

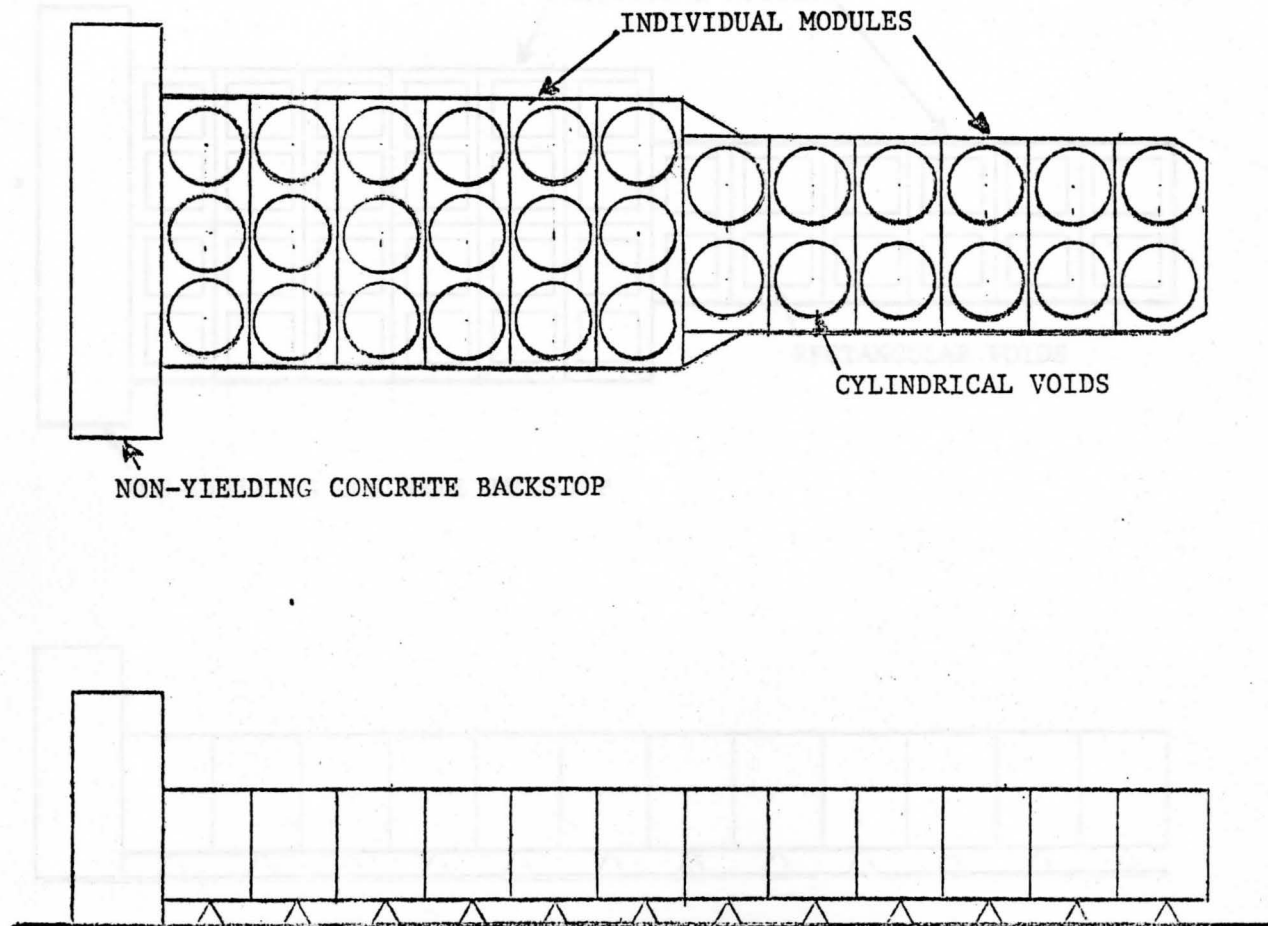


FIGURE 2.13
TEXAS TRANSPORTATION INSTITUTE CRASH CUSHION WITH CYLINDRICAL VOIDS

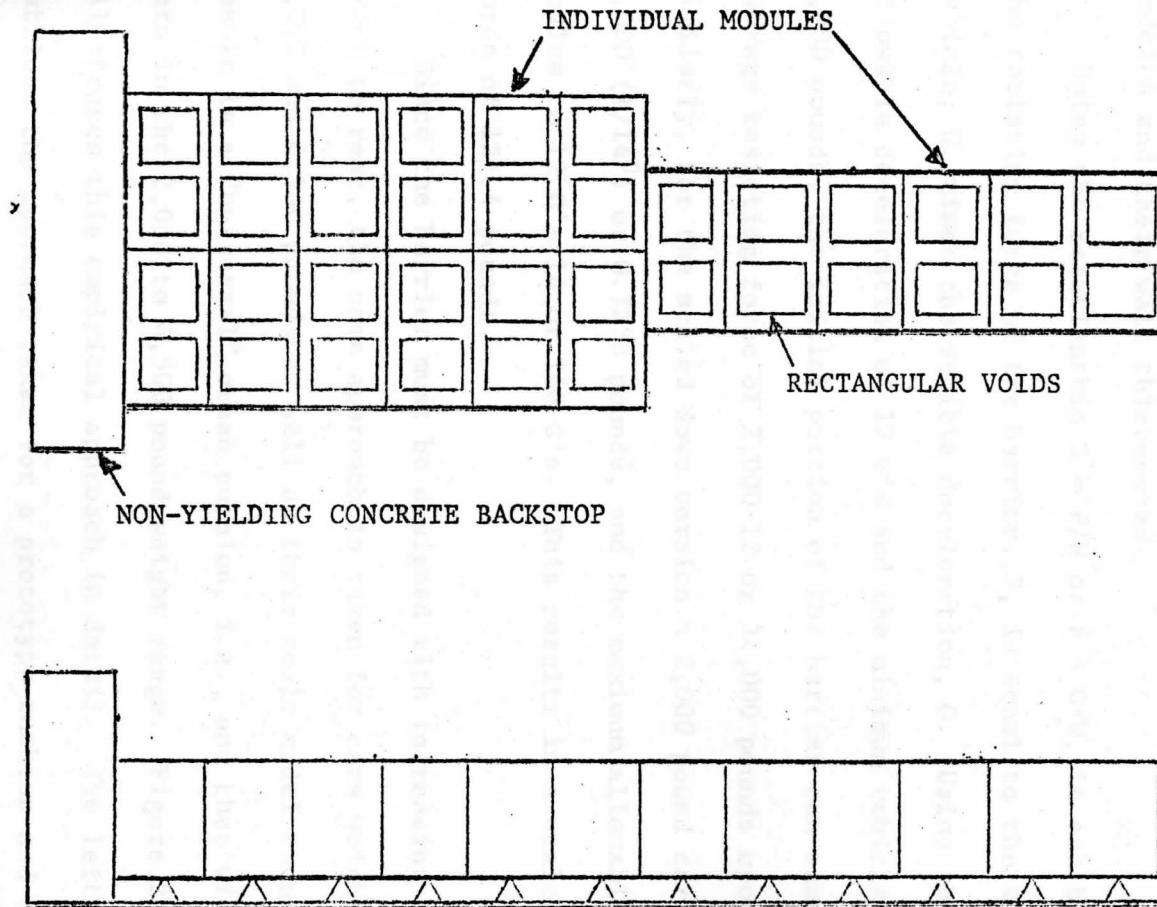


FIGURE 2.14
BASIC CRASH CUSHION WITH RECTANGULAR VOIDS

Next, using the laws of similitude and the work-energy approach to crash cushion design, an investigation was made to determine the resisting force and energy absorption characteristics of the crash cushion modules both in full and 1/14 scale versions. This step was necessary in order to empirically determine the overall size of the modules and their wall thicknesses.

Using the relationship $G = F/W$ or $F = G \cdot W$, it can be seen that the resisting force of the barrier, F , is equal to the weight of the vehicle, W , times the vehicle deceleration, G . Using the maximum allowable deceleration of 12 G's and the minimum vehicle weight of 2,000 pounds, the initial portion of the barrier can exert a maximum average resisting force of $2,000 \cdot 12$ or 24,000 pounds upon impact. Similarly, for the scaled down version a 2,000 pound car weighs $2,000 (1/14^3)$ or 0.7228 pounds, and the maximum allowable deceleration scales to $12 G's \cdot 14$ or 168 G's. This results in a scale model barrier force of 121.4 pounds.

Since the barrier must be designed with increasing stiffness from front to rear, the same approach is taken for cars weighing 3,000, 4,000 and 4,500 pounds as well as their scale model counterparts. The result is a "universal" crash cushion, i.e., one that will safely stop cars in the 2,000 to 4,500 pound weight range. Figure 2.15 further illustrates this empirical approach in detail. The left hand column outlines the approach taken for a prototype cushion and in the right hand column are the corresponding figures for a 1/14 scale model cushion. The weights shown are vehicle weights; the kinetic energy (KE) is the energy that each section of the barrier must dissipate;

	PROTOTYPE		MODEL
Weight of Vehicle (lb.)	2,000.00		0.728
K.E. of Vehicle (ft.-lb.)	240,000.00	SECTION	87.630
Energy Abs. by this Sect.(ft.-lb.)	240,000.00	1	87.140
Max. Force (lb.)	24,000.00		122.450
Actual Length of this Section(ft.)	12.50		0.892
Weight of Vehicle (lb.)	3,000.00		1.093
K.E. of Vehicle (ft.-lb.)	360,000.00	SECTION	131.200
Energy Abs. by this Sect.(ft.-lb.)	120,000.00	2	43.570
Max. Force (lb.)	36,000.00		183.670
Actual Length of this Section(ft.)	4.17		0.297
Weight of Vehicle (lb.)	4,000.00		1.457
K.E. of Vehicle (ft.-lb.)	480,000.00	SECTION	174.920
Energy Abs. by this Sect.(ft.-lb.)	120,000.00	3	43.570
Max. Force (lb.)	48,000.00		244.900
Actual Length of this Section(ft.)	3.13		0.224
Weight of Vehicle (lb.)	4,500.00		1.639
K.E. of Vehicle (ft.-lb.)	540,000.00	SECTION	196.790
Energy Abs. by this Sect.(ft.-lb.)	60,000.00	4	21.870
Max. Force (lb.)	54,000.00		275.500
Actual Length of this Section(ft.)	1.39		0.099
Total Length (ft.)	21.19		1.510

FIGURE 2.15
EMPIRICAL DESIGN OF "UNIVERSAL" CRASH CUSHION

and the maximum force is the force that each section can exert without exceeding the 12 G force limit. The minimum length of each section is obtained by dividing the kinetic energy by the maximum force. The crush ratio is the amount of deformation that a module will undergo before bottoming out and can be found by dividing the amount of deformation by the original length. A crush ratio of 0.8 as tentatively selected based upon a review of published test results⁽¹⁷⁾ and some preliminary model tests made in this investigation. The actual lengths given in Figure 2.15 were obtained by dividing the minimum length by the crush ratio.

Theoretically, in full scale, section 1 will completely stop a 2,000 pound car. A 3,000 pound car will pass through section 1, expending 240 kip-ft of kinetic energy as it does. Section 2 will then dissipate the remainder of the 360 kip-ft of kinetic energy that a 3,000 pound car travelling at 60 mph initially possesses. Likewise, sections 3 and 4 will stop 4,000 and 4,500 pound cars respectively.

The next step was to construct a series of prototype and scale model modules with rectangular voids. Through construction of a prototype module, observations could be made on its structural integrity during casting, handling, and installation. Also, static tests conducted on the prototype would yield information about the peak load, static energy absorption, and fracture pattern during crushing. Through the construction of scale model modules, the validity of the similitude approach previously used could be confirmed. The successful scaling of peak load, energy absorption, and fracture pattern must be accomplished before any further progress could be made.

From Figure 2.15 it can be seen that the prototype module used in the front part of the cushion must be capable of exerting a 24,000 pound average resisting force on an impacting vehicle. It should be emphasized that this is a 24,000 pound dynamic force which should not be confused with the resisting force that would be developed by the same module subjected to quasi-static loading in the laboratory. This difference in resisting forces will be referred to as a dynamic:static load factor and is a function of the rate at which the load is applied.

The Texas Transportation Institute conducted a limited study⁽¹⁷⁾ on scale model crash modules. The results of two full scale crash tests were compared with the predicted energy absorption obtained from laboratory static tests on individual modules. The dynamic:static factors obtained in this test were 1.77 and 1.39, giving an average of 1.58. Based on these findings, a dynamic:static load factor of 1.5 was initially selected for this study. Therefore, a prototype module was needed that would exert $24,000/1.5$ or 16,000 pounds of average static resisting force and a 1/14 scale model module exerting $121.4/1.5$ or 80.93 pounds of average static resisting force.

The overall dimensions of the prototype module were arrived at from a study of existing crash cushion designs. An overall width of 40 inches, a height of 36 inches and a length of 21 inches made the module small enough to be handled by two men. The only remaining parameter to be established in order to develop 16,000 pounds of average resisting force was the module wall thickness. It seemed logical that the wall thickness would be dependent on the type of material used. Therefore, this parameter would have to be established

for each type of lightweight concrete being considered for use.

For the first series of tests, Dycon-2 concrete was used because of its favorable performance in the initial feasibility study conducted by Bakos.⁽¹⁾ A number of scale model modules were then constructed with their overall dimensions being properly scaled down. The wall thickness was varied in an attempt to find a module that would exert the necessary 80.93 pounds of average static resisting force. These model modules were constructed by casting a large slab of concrete and then cutting the module to the proper size from this slab. This technique was employed to insure a uniform concrete matrix and to eliminate any edge effects from casting. From these initial tests, it was established that a wall thickness of 5/32 in. was necessary to sustain an average resisting force of 80 pounds. Then, from the laws of similitude, a prototype module with a wall thickness of $5/32 \cdot 14$ or $2 \frac{3}{16}$ in. should be capable of developing 16,000 pounds of average resisting force. Two prototype modules were then constructed to test this theory.

To construct a prototype module, a box shaped plywood mold was fabricated. The rectangular void spaces were accomplished by constructing box-shaped inner walls from one-inch thick styrofoam boards. The concrete was then poured into the mold between the styrofoam inner walls and the plywood outer walls. Details of construction are illustrated in Figures 2.16 to 2.19. It should be noted that all mix design procedures were taken from the initial study by Bakos.⁽¹⁾ Part B gives details of the lightweight concrete mixes used herein. The plywood forms were removed after 24 hours and the



FIGURE 2.16
PLACING STYROFOAM SHEETS
TO FORM RECTANGULAR VOIDS



FIGURE 2.17
STYROFOAM IN PLACE



FIGURE 2.18
POURING LIGHTWEIGHT CONCRETE INTO
MOLD FOR PROTOTYPE MODULE



FIGURE 2.19
PROTOTYPE MODULE MOLD AFTER
CONCRETE HAS BEEN POURED



FIGURE 2.20
RELATIVE SIZE OF
PROTOTYPE AND MODEL DYCON-2 MODULES

corresponding loads by $(14)^2$. By so doing, the values of load and displacement for the model modules should theoretically match the values extracted from the prototype module curves.

In Table 2.13 the load ordinates for the prototype and model modules presented in Table 2.12 were averaged and tabulated. The standard deviation (S.D.) for each model ordinates was also calculated and tabulated. The next step was to plot curves of the average load versus deflection for the prototype and model modules. Figure 2.23 presents the plotted data from Table 2.13. Upon examination of these curves, along with observations made during the static compression tests, it was concluded that the behavior of the Dycon-2 model modules, with respect to static compressive strength and mode of failure, duplicates the performance of the prototype modules with sufficient accuracy. It should be noted that the module material itself, namely low-density concrete, imposes limitations on any form of reproducibility.

With the static performance of the Dycon-2 module successfully modeled, the same approach was applied to modules made of Perlite 4. From preliminary tests conducted on the Perlite, it was established that a wall thickness of 3/16 in. was necessary to develop the 80.93 pound average resisting force necessary for the model barrier. This meant that a corresponding prototype module having a 2 5/8 in. wall thickness should be sufficient to develop the required 16,000 pound average resisting force. Casting a prototype module from Perlite concrete uncovered some undesirable traits with respect to the structural integrity of the module. Shrinkage cracks developed in



FIGURE 2.21
STATIC COMPRESSION YIELD OF DYCON-2
PROTOTYPE MODULE

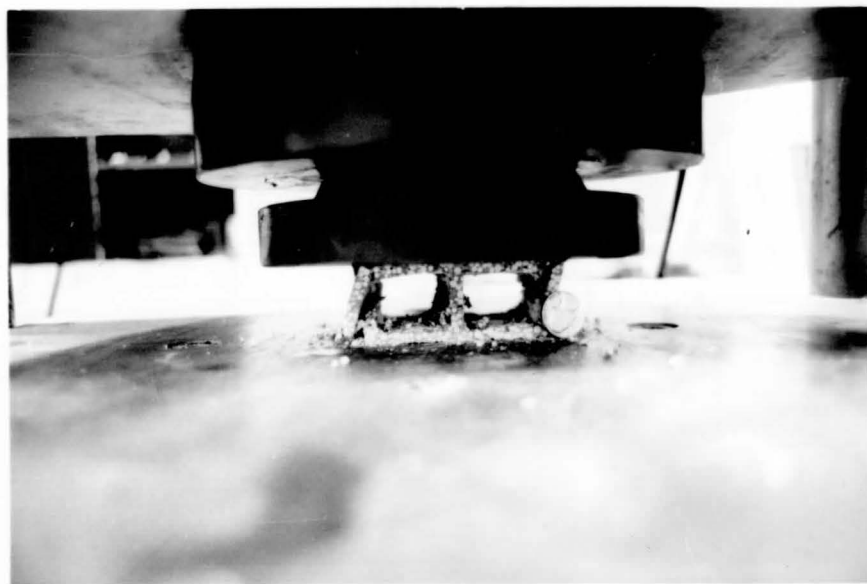


FIGURE 2.22
STATIC COMPRESSION YIELD OF DYCON-2
MODEL MODULE

DISP(in.)	LOAD (kips)											
	P1	P2	M1	M2	M3	M4	M5	M6	M7	M8	M9	M10
0.25	21.40	22.50	24.50	22.90	23.80	24.10	26.50	23.40	24.70	27.40	24.80	22.00
0.50	22.50	23.10	25.10	22.75	23.20	22.40	24.75	23.00	23.40	24.00	25.60	23.20
0.75	22.70	26.10	24.40	21.60	22.30	21.90	23.60	22.60	22.10	21.60	22.60	21.70
1.00	21.80	23.00	21.70	21.00	22.00	20.60	21.60	17.40	20.30	18.20	19.10	20.60
1.25	18.60	22.40	18.25	19.70	18.60	20.25	19.30	17.00	19.50	18.00	17.70	18.30
1.50	17.00	21.00	18.31	16.40	18.00	20.12	18.00	16.50	17.30	17.60	16.75	17.00
2.00	17.00	15.70	18.18	16.00	17.50	19.80	17.50	16.25	17.00	17.50	16.00	16.75
3.00	14.00	13.20	16.70	15.75	16.00	17.50	17.00	15.70	16.20	15.40	14.80	16.00
4.00	13.00	12.40	16.00	14.70	15.25	14.30	16.20	15.10	15.60	15.25	13.40	15.80
5.00	13.75	14.75	14.20	12.25	14.70	14.00	13.90	14.60	13.60	14.20	13.00	14.70
6.00	15.00	14.50	13.90	12.25	14.00	11.10	12.20	15.60	13.10	14.70	14.20	14.30
7.00	16.50	14.00	13.60	12.00	13.75	12.25	12.80	16.70	14.30	15.00	15.10	14.60
8.00	16.50	14.50	15.25	11.70	14.50	13.70	15.80	17.00	16.25	15.75	16.10	15.30
9.00	16.00	17.00	16.00	13.50	16.30	15.50	16.20	17.20	16.80	15.90	17.40	17.10
10.00	19.25	18.50	16.50	15.10	18.60	17.00	17.90	18.40	19.50	18.70	19.20	18.00
11.00	20.25	20.00	18.00	19.70	21.50	18.70	19.00	21.40	20.70	19.80	19.30	21.00

TABLE 2.12
LOAD VS. DISPLACEMENT VALUES FOR DYCON-2 MODULES

DISPLACEMENT (in.)	PROTOTYPE LOAD (kips)		MODEL LOAD (kips)	
	\bar{x}		\bar{x}	S.D.
0.25	21.95		24.41	1.60
0.50	22.80		23.74	1.08
0.75	24.40		22.44	.92
1.00	22.40		20.25	1.54
1.25	20.50		18.66	1.01
1.50	19.00		17.60	1.11
2.00	16.35		17.25	1.15
3.00	13.60		16.11	.79
4.00	12.70		15.60	.85
5.00	14.25		13.92	.79
6.00	14.75		13.54	1.36
7.00	15.25		14.01	1.44
8.00	15.50		15.14	1.52
9.00	16.50		16.19	1.13
10.00	18.88		17.89	1.34
11.00	20.13		19.91	1.20

TABLE 2.13
 AVERAGE LOAD VS. DISPLACEMENT
 VALUES FOR DYCON-2 MODULES

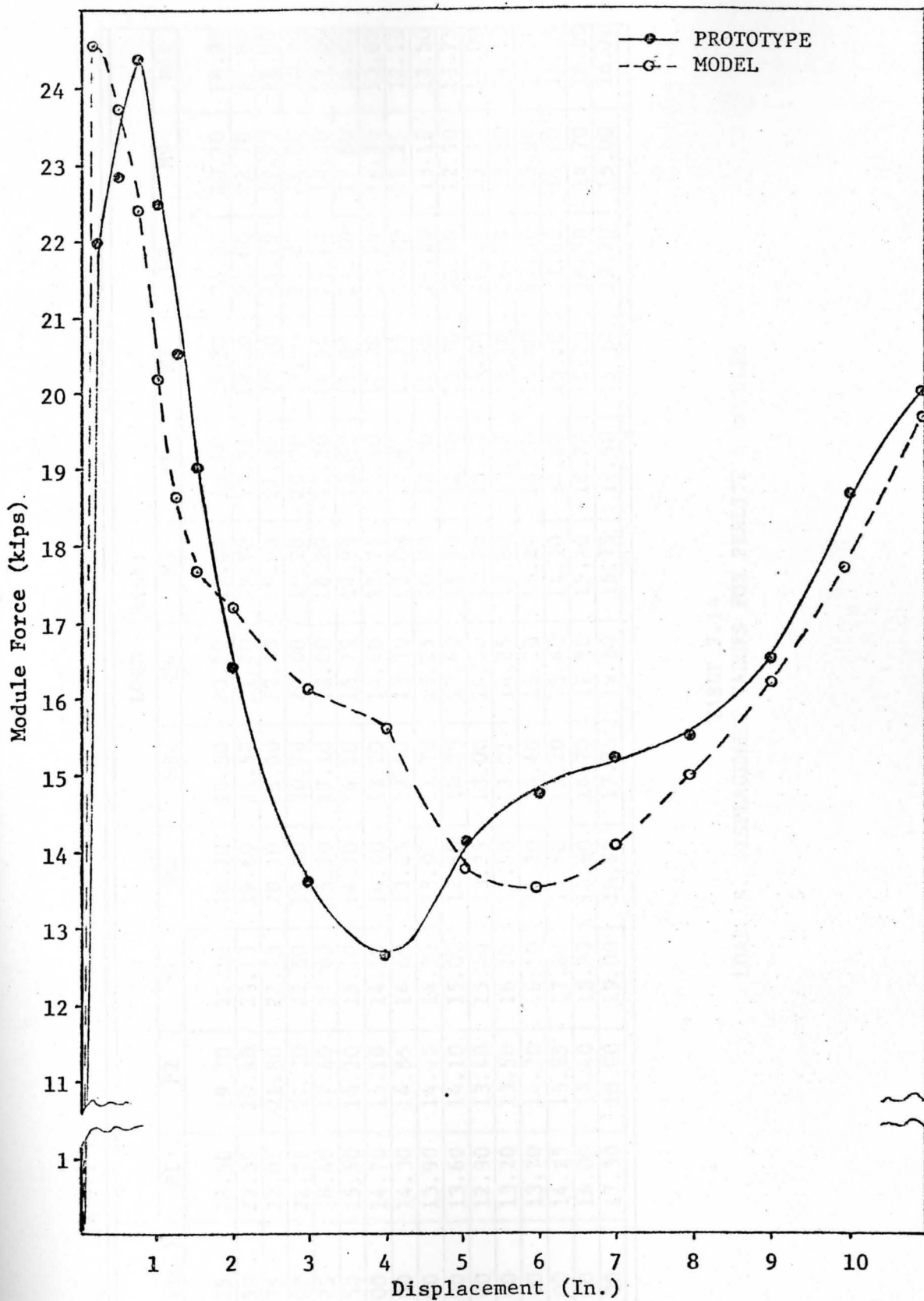


FIGURE 2.23
FORCE-DISPLACEMENT CURVE FOR DYCON-2
PROTOTYPE AND MODEL MODULES

DISP (in.)	LOAD (kips)											
	P1	P2	M1	M2	M3	M4	M5	M6	M7	M8	M9	M10
0.25	18.50	19.70	21.10	18.70	19.30	20.10	18.40	19.60	19.30	20.20	20.70	18.90
0.50	22.50	20.40	23.10	19.60	21.50	21.70	19.90	20.75	19.80	20.80	22.70	21.60
0.75	22.00	21.80	22.75	20.10	21.60	22.40	19.60	21.20	20.20	21.70	22.50	22.00
1.00	22.70	21.20	22.50	19.80	20.70	22.00	19.20	20.00	19.50	21.20	21.80	20.90
1.25	18.40	17.60	17.60	15.50	17.10	18.00	16.20	15.20	14.90	16.10	18.20	17.60
1.50	15.50	16.20	15.20	14.70	14.10	15.75	14.90	13.80	13.00	14.80	17.60	14.80
2.00	14.70	15.10	14.50	14.00	13.20	14.40	12.75	13.00	12.20	13.66	14.80	13.00
3.00	14.30	14.65	14.60	13.25	12.40	13.30	12.00	12.80	11.75	13.70	12.25	12.10
4.00	13.90	14.25	14.75	13.00	11.70	13.25	10.80	12.00	11.25	14.20	13.10	12.50
5.00	13.60	14.10	15.00	12.80	12.25	13.60	11.70	12.90	13.70	15.40	12.90	13.75
6.00	12.90	13.40	15.40	13.25	13.00	14.10	12.75	13.25	14.00	16.10	13.25	14.00
7.00	13.20	13.50	16.10	13.50	13.71	14.25	12.80	13.62	14.10	16.70	13.80	14.10
8.00	13.70	14.70	16.50	14.20	14.40	15.10	13.20	14.00	14.80	17.10	13.90	15.10
9.00	14.25	15.85	17.80	14.80	15.20	15.60	14.10	14.80	15.20	17.60	14.00	15.25
10.00	16.00	16.40	18.20	15.60	16.70	17.80	15.20	16.70	15.20	18.50	14.70	16.00
11.00	17.50	18.00	19.00	16.80	17.75	19.10	15.75	17.50	15.20	19.70	15.00	16.70

TABLE 2.14
LOAD VS. DISPLACEMENT VALUES FOR PERLITE 4 MODULES

DISPLACEMENT (in.)	PROTOTYPE LOAD (kips)		MODEL LOAD (kips)	
	\bar{x}		\bar{x}	S.D.
0.25	19.10		19.63	.88
0.50	21.45		21.15	1.20
0.75	21.90		21.40	1.10
1.00	21.96		20.76	1.12
1.25	18.00		16.64	1.21
1.50	15.85		14.87	1.23
2.00	14.90		13.55	.86
3.00	14.48		12.82	.89
4.00	14.08		12.66	1.26
5.00	13.85		13.40	1.15
6.00	13.15		13.91	1.08
7.00	13.35		14.27	1.20
8.00	14.20		14.83	1.21
9.00	15.05		15.44	1.30
10.00	16.20		16.46	1.35
11.00	17.75		17.25	1.66

TABLE 2.15
 AVERAGE LOAD VS. DISPLACEMENT
 FOR PERLITE 4 MODULES

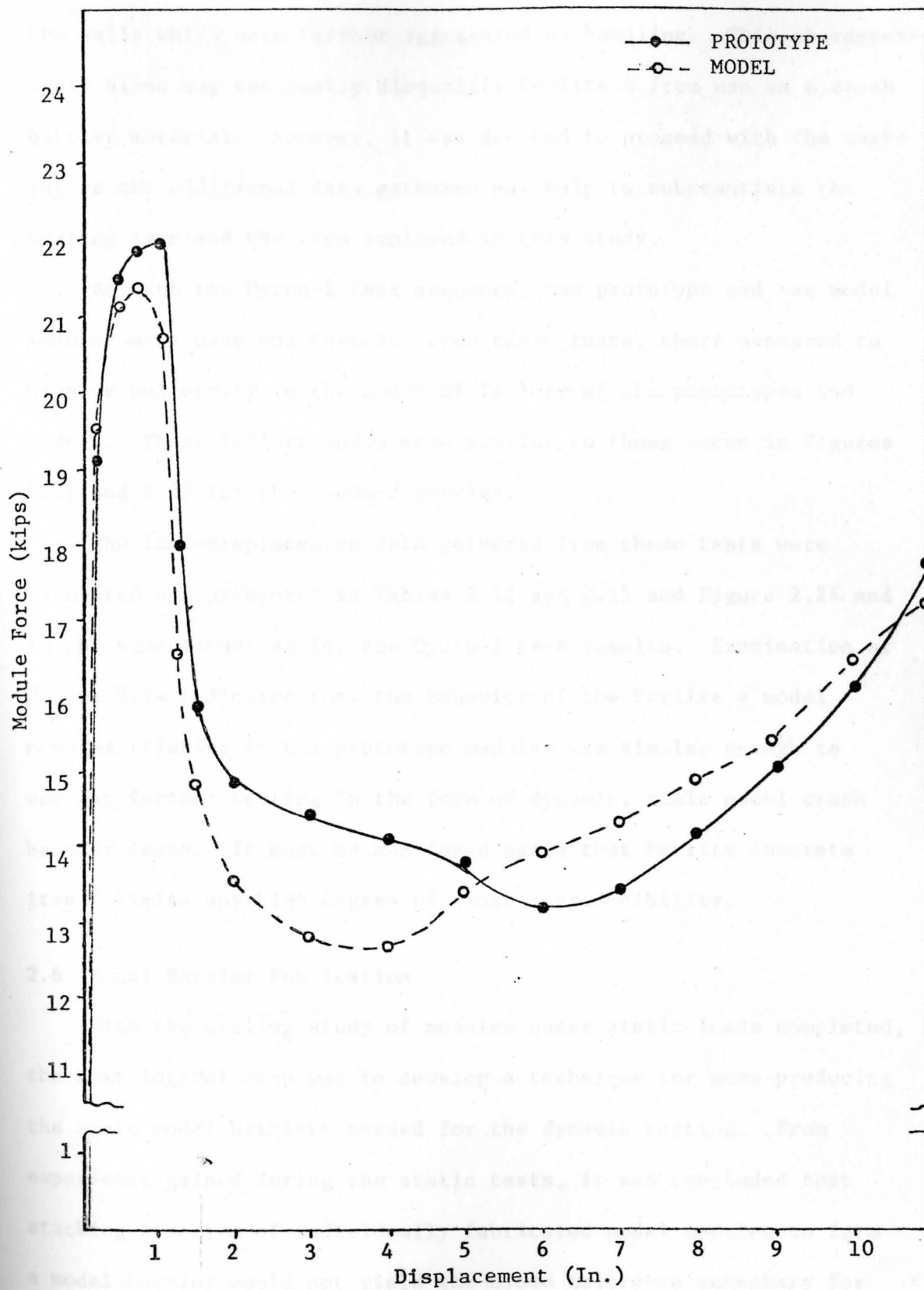


FIGURE 2.24
FORCE-DISPLACEMENT CURVE FOR PERLITE-4
PROTOTYPE AND MODEL MODULES

the walls which were further aggravated by handling. This characteristic alone may eventually disqualify Perlite 4 from use as a crash barrier material. However, it was decided to proceed with the testing as the additional data gathered may help to substantiate the scaling laws and theories employed in this study.

As with the Dycon-2 test sequence, two prototype and ten model modules were made and tested. From these tests, there appeared to be some uniformity in the modes of failure of the prototypes and models. These failure modes were similar to those shown in Figures 2.21 and 2.22 for the Dycon-2 modules.

The load-displacement data gathered from these tests were tabulated and presented in Tables 2.14 and 2.15 and Figure 2.24 and in the same manner as for the Dycon-2 test results. Examination of Figure 2.24 indicates that the behavior of the Perlite 4 model modules relative to the prototype modules was similar enough to warrant further testing in the form of dynamic, scale model crash barrier tests. It must be mentioned again that Perlite concrete itself limits any high degree of exact reproducibility.

2.6 Model Barrier Fabrication

With the scaling study of modules under static loads completed, the next logical step was to develop a technique for mass producing the scale model barriers needed for the dynamic testing. From experience gained during the static tests, it was concluded that stacking a series of individually fabricated model modules to form a model barrier would not yield the close tolerance necessary for this phase of the testing. A method of construction was devised

where the barrier sidewalls would be made from thin sheets and then bonded to the inner walls. An exploded view of the necessary pieces for a Dycon-2 scale model barrier is shown in Figure 2.25. The same barrier when bonded together using epoxy is shown in Figure 2.26.

The question arose as to whether gluing the modules together would have any effect on its performance as opposed to casting the modules from one piece. A series of individual scale model modules were made from Dycon-2 concrete using the glued wall technique. They were individually crushed and the results were compared with the model module results given in Table 2.13. The curve in Figure 2.27 compares the load-displacement curves for glued-wall and cast model individual modules. The glued wall technique appeared to have no effect on the individual model module's performance.

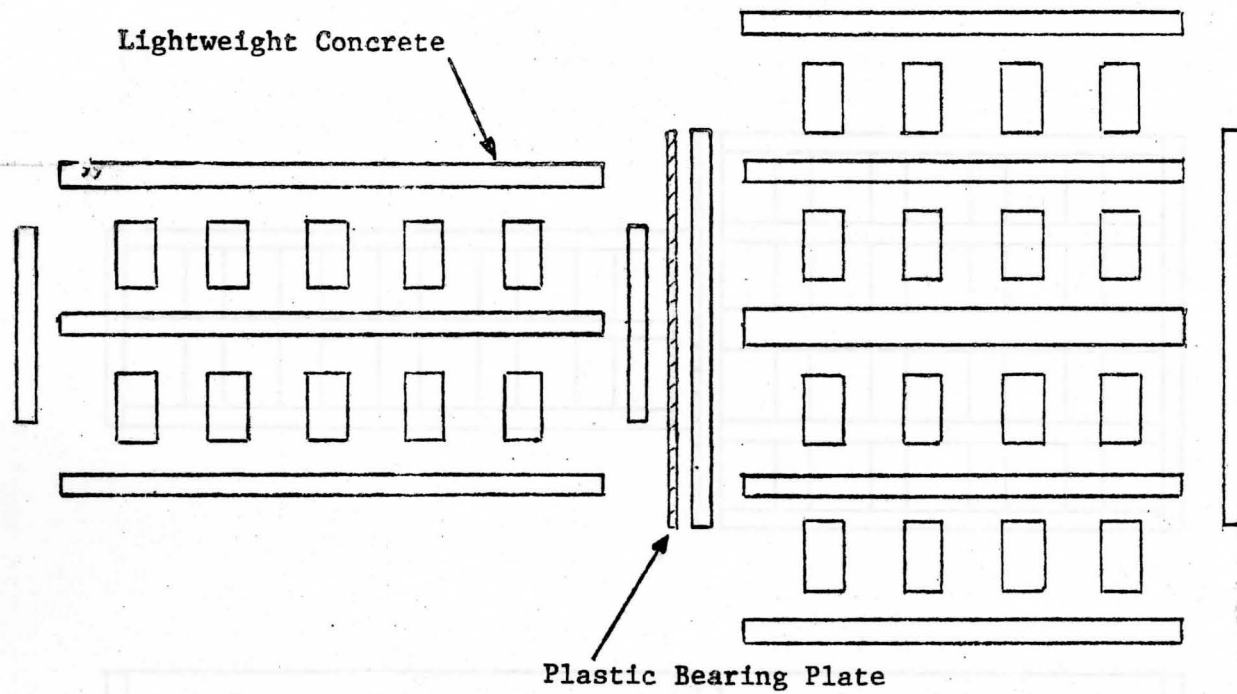


FIGURE 2.25
EXPLODED VIEW OF SCALE MODEL CRASH BARRIER PARTS

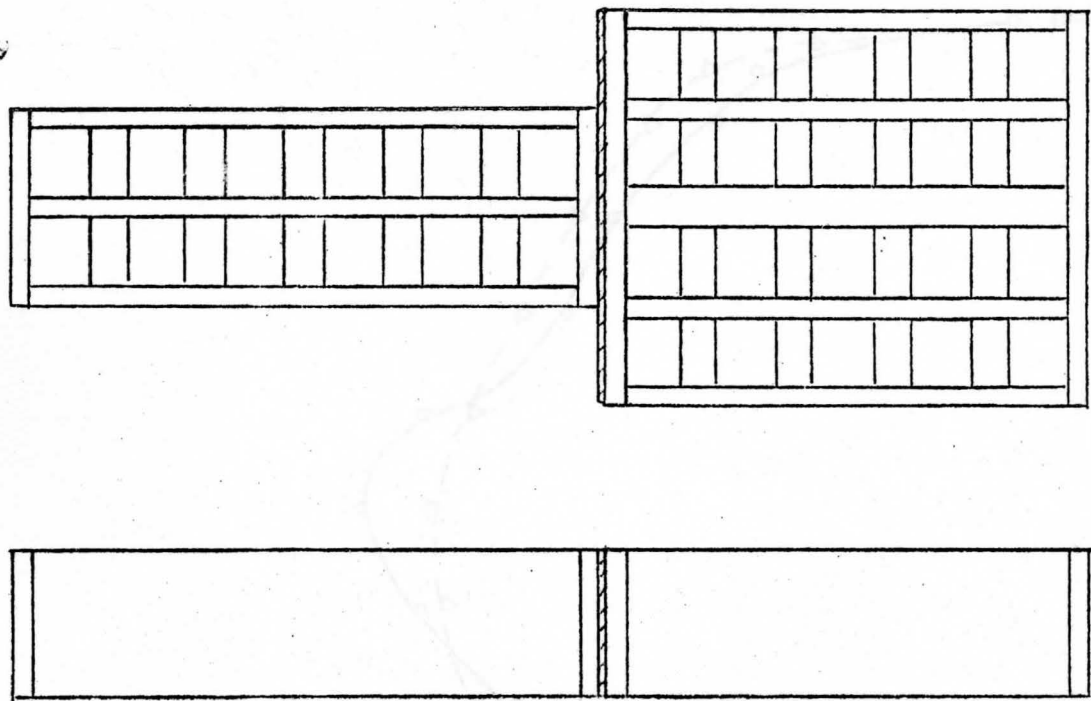


FIGURE 2.26
COMPLETED SCALE MODEL CRASH CUSHION.

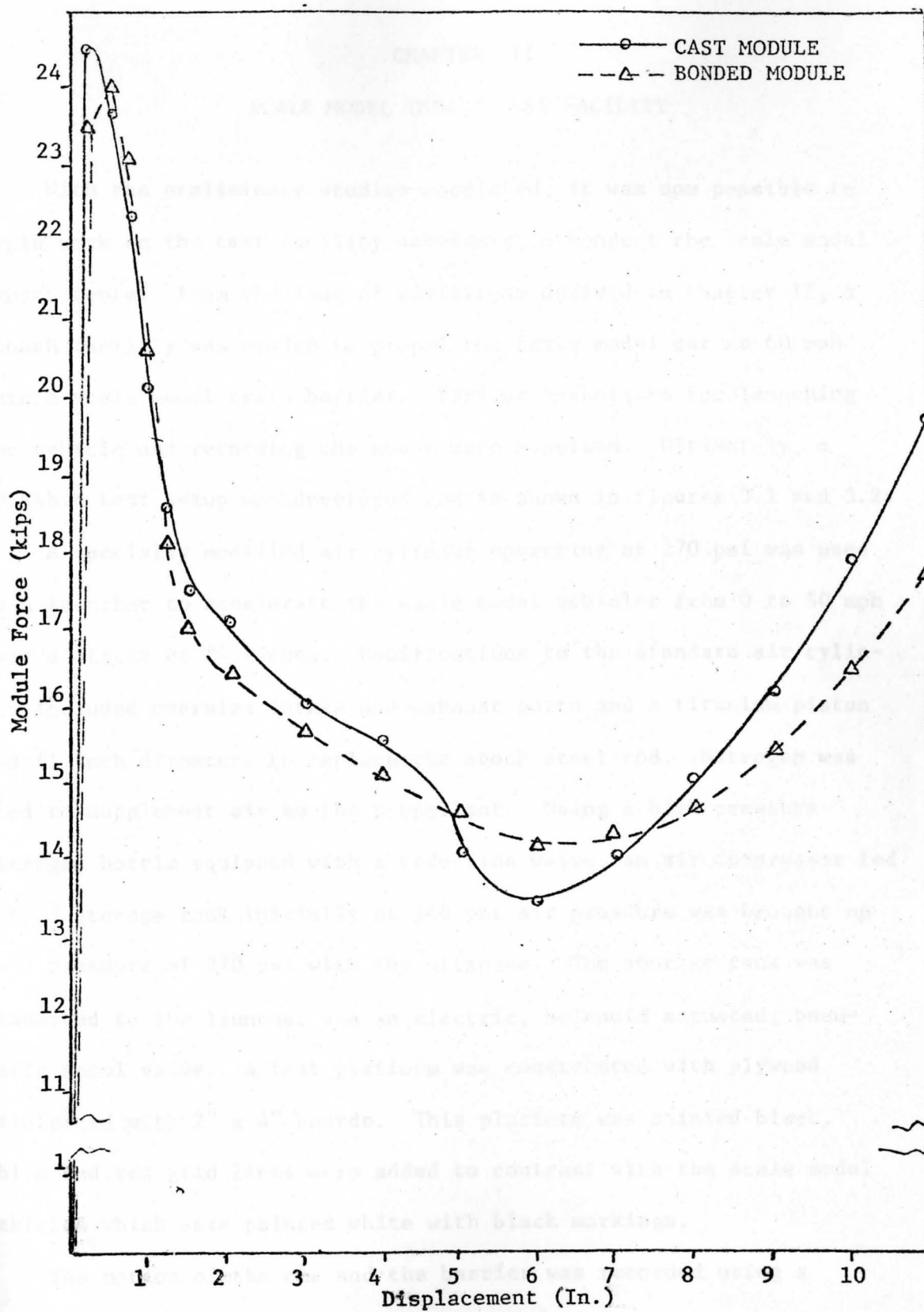


FIGURE 2.27
 FORCE-DISPLACEMENT CURVE FOR CAST AND BONDED
 DYCON-2 SCALE MODEL MODULES

CHAPTER III

SCALE MODEL IMPACT TEST FACILITY

With the preliminary studies completed, it was now possible to begin work on the test facility necessary to conduct the scale model impact tests. From the laws of similitude derived in Chapter II, a launch facility was needed to propel the scale model car at 60 mph into a scale model crash barrier. Various techniques for launching the vehicle and recording the event were examined. Ultimately, a workable test setup was developed and is shown in Figures 3.1 and 3.2.

A specially modified air cylinder operating at 270 psi was used as a launcher to accelerate the scale model vehicles from 0 to 60 mph over a stroke of 24 inches. Modifications to the standard air cylinder included oversize intake and exhaust ports and a titanium piston rod (1 inch diameter) to replace the stock steel rod. Nitrogen was used to supplement air as the propellant. Using a high pressure nitrogen bottle equipped with a reduction valve, an air compressor fed 2 ft.³ storage tank initially at 160 psi air pressure was brought up to a pressure of 270 psi with the nitrogen. The storage tank was connected to the launcher via an electric, solenoid actuated, pneumatic spool valve. A test platform was constructed with plywood reinforced with 2" x 4" boards. This platform was painted black. White and red grid lines were added to contrast with the scale model vehicles which were painted white with black markings.

The motion of the car and the barrier was recorded using a 35 mm high speed, Fastax motion picture camera.* The camera was

*See Appendix B for detailed information on equipment.

mounted overhead to record the plan view of the collision. It was operated at a speed of 1,000 frames per second.

A timing station was set up to electronically measure the impact velocity of the scale model cars. This was accomplished by mounting a pair of photoelectric cells adjacent to the test track and just in front of the impact interface. Two laser beams were used as light sources to trigger the photocells. The laser beams were positioned so that their beams would be parallel and would span the track in a direction perpendicular to the movement of the test vehicles. As the scale model vehicle passed by each of the two fixed photocells, the laser beams would be broken and the time lapse between the first and second photocells was recorded using a Tektronix Universal Counter/Timer. Knowing the perpendicular distance between the laser beams and the time lapse from the two photocells connected to the timer, the initial impact velocity could be calculated. This velocity was eventually compared with the computed velocity obtained by analyzing the film data from the high speed motion picture camera.

The film taken from the camera after each test run was processed in an electric Micro Recorder film processor. The film was analyzed by projecting it onto a large screen and physically measuring the relative displacement of the vehicle frame by frame. Then, knowing the relative displacement of the vehicle from frame to frame and the time lapse between frames, it was possible to compute the instantaneous velocity, deceleration, and G-force of the scale model car as it was being brought to rest by the crash barrier. A computer program was written to take the time and relative displacement data, apply the

FIGURE 3.1
SCALE MODEL
IMPACT TEST
FACILITY

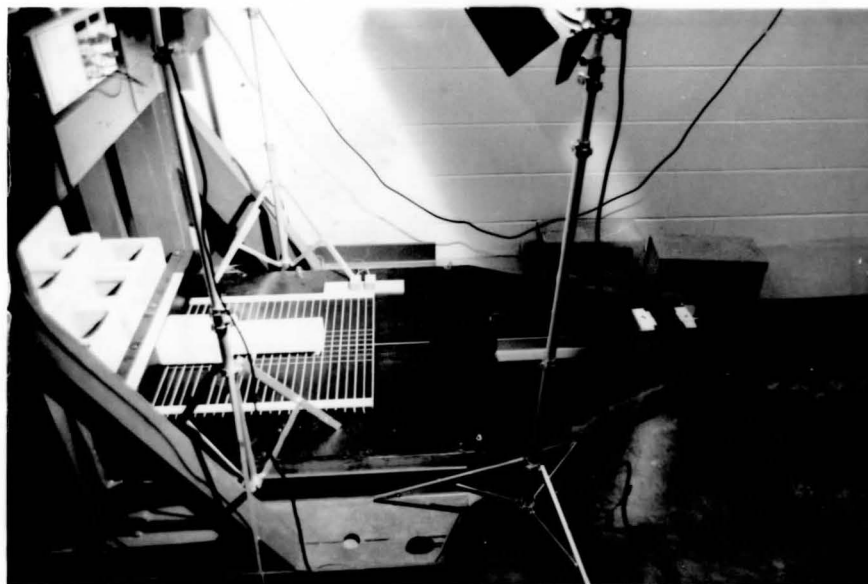
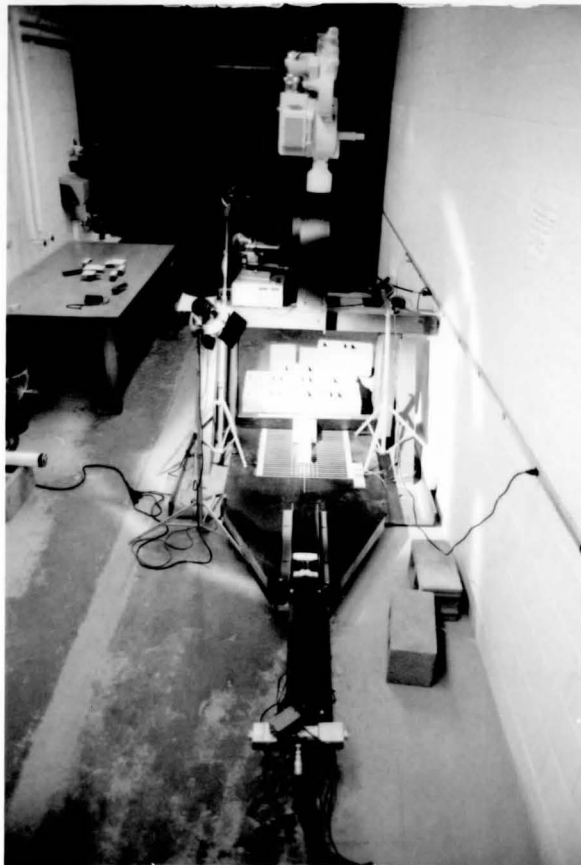


FIGURE 3.2
CRASH CUSHION AND VEHICLE IN PLACE BEFORE TEST

appropriate scale factors, and compute prototype values of time, displacement, velocity, deceleration, and G-force. This program, which was written in "Basic" language, is shown in Figure 3.3.

```

10 INPUT "N="
20 DAT DIM, AT=0
30 DAT V(2,1)=0
40 DAT A(2,1)=0
50 PRINT "LIBRARY INPUT"
60 DAT LIBRARY "C:\PROGRAMS\LIBRARY"
70 PRINT "LIBRARY TIME"
80 INPUT T1
90 T=0
100 DIM S(1), V(1), A(1), G(1)
110 V(1,1)=0
120 V(1,2)=0
130 FOR I=1 TO 2
140 A(I,1)=0
150 A(I,2)=(V(I,2)-V(I,1))/T1
160 G(I,1)=A(I,1)/9.8
170 G(I,2)=A(I,2)/9.8
180 V(1,1)=V(1,1)+A(1,1)*T1
190 V(1,2)=V(1,2)+A(1,2)*T1
200 A(1,1)=A(1,1)+A(1,1)
210 A(1,2)=A(1,2)+A(1,2)
220 G(1,1)=G(1,1)+G(1,1)
230 G(1,2)=G(1,2)+G(1,2)
240 PRINT "CONTINUE?"
250 INPUT "Y/N"
260 IF Y=1 THEN GOTO 20
270 END

```

FIGURE 3.3
COMPUTER PROGRAM TO ANALYZE FILM DATA

```
10 DIM D(30,1),V(30,1),A(30,1)
20 PRINT 'INPUT NO. ROWS'
30 INPUT R
40 MAT D(R,1)=(0)
50 MAT V(R,1)=(0)
60 MAT A(R,1)=(0)
70 PRINT 'INPUT D MATRIX'
80 MAT INPUT D
90 PRINT 'INPUT TIME INCREMENT'
100 INPUT T1
110 L=T1*12
120 D1=0
130 T=0
140 PRINT 'TIME', 'DIS', 'VEL', 'ACC', 'G-FORCE'
150 V(1,1)=D(1,1)/L
160 V1=V(1,1)
170 PRINT '0', '0', V1, '*', '*'
180 FOR Z= 2 TO R
190 V(Z,1)=D(Z,1)/L
200 A(Z,1)=(V(Z,1)-V(Z-1,1))/T1
210 G=A(Z,1)/32.2
220 D1=D1+D(Z,1)
230 V1=V(Z,1)
240 A1=A(Z,1)
250 T=T+T1
260 PRINT T*14, D1*14/12, V1, A1/14, G/14
270 NEXT Z
280 PRINT 'CONTINUE ?'
290 INPUT Y
300 IF Y=1 GOTO 20
310 END
```

FIGURE 3.3
COMPUTER PROGRAM TO ANALYZE FILM DATA

CHAPTER IV
IMPACT TEST RESULTS AND DISCUSSION

This chapter presents the results from twelve successful scale model impact tests. Although a total of 22 tests were conducted, not all of these were a success because of technical problems during the testing and the film processing. During the initial impact tests, observations were made to determine the barrier's mode of failure during impact. The film strip shown in Figure 4.1 shows a Dycon-2 scale model crash barrier being impacted by a scale model 2,000 pound vehicle. This sequence of photographs indicates that each

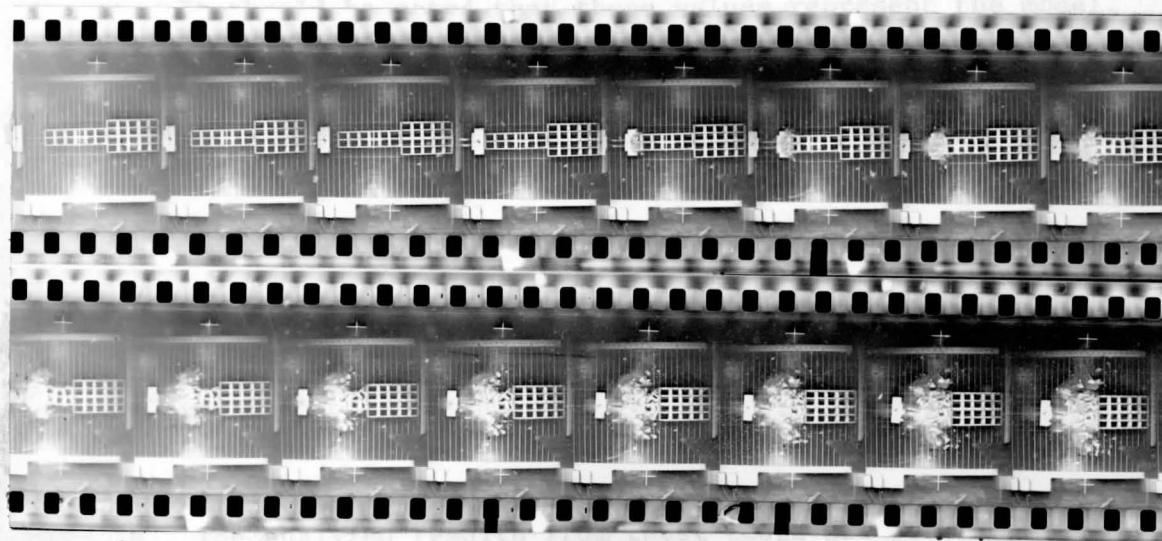


FIGURE 4.1
DYCON-2 BARRIER IMPACTED BY "2,000 POUND" VEHICLE

barrier module behaved as an integral unit, thereby producing a very controlled and desirable response mechanism for the entire system upon impact. After these initial three tests, modifications were made, i.e., thicker barrier walls were used in successive models and a bearing plate was added, as shown in Figures 2.25 and 2.26, to improve the barrier performance with respect to deceleration when impacted by a "4,500 pound" scale model vehicle.

Data from the twelve aforementioned successful tests was generated by extracting the relative displacement of the crash vehicle per frame from the highspeed film strips similar to that shown in Figure 4.1. Time marks exposed in the film strip permitted the conversion from displacement/frame to displacement/second. The computer program shown in Figure 3.3 was then employed to analyze the film data and to tabulate the time (seconds), displacement (ft.), velocity (ft/sec), deceleration (ft/sec²), and G-force (G's) for each test vehicle during impact. It should be noted that these values represent the model values scaled up to prototype values and were obtained directly from the computer output. Therefore, *all of the data from the scale model tests will be presented in terms of prototype values.* For example, Figure 4.2 gives the computer output for the Dycon-2 barrier response during impact by the "2,000 pound" model car shown in Figure 4.1.

Of the successful tests, five runs were made using identical Dycon-2 scale model barriers and the "4,500 pound" scale model impact vehicle. The analyzed results from these tests are presented in Table 4.1 and the apparent consistency of the results was thought to be sufficient to eliminate the need for continued repetitious tests.

TIME	DIS	VEL	ACC	G-FORCE
0	0	90.64392	*	*
2.085081E-02	1.761666	84.48911	-295.1831	-9.167184
4.170163E-02	3.43	80.01286	-214.6794	-6.667063
6.255239E-02	4.888333	69.9413	-483.0295	-15.00092
8.340317E-02	6.195	62.66739	-348.8547	-10.834
.1042539	7.288166	52.42799	-491.0786	-15.25089
.1251947	8.233166	45.32196	-340.8035	-10.58396
.1459555	8.962332	34.97064	-496.4463	-15.41759
.1668063	9.545666	27.97652	-335.4363	-10.41728
.1876571	10.05608	24.47945	-167.7186	-5.208652
.2085078	10.49358	20.98239	-167.7179	-5.20863
.2293586	10.85817	17.48532	-167.7186	-5.208652
.2502094	11.14983	13.98826	-167.7182	-5.208638
.2710602	11.368	10.46322	-169.0602	-5.250316
.2919109	11.54066	8.28105	-104.6562	-3.250193
.3127617	11.6865	6.99413	-61.72034	-1.91678
.3336125	11.795	5.203632	-85.87183	-2.666826
.3544633	11.795	0	-249.5649	-7.750463

FIGURE 4.2
TABULATED IMPACT TEST DATA

TEST	IMPACT VELOCITY (ft/sec)	BARRIER DISPLACEMENT (STOPPING DISTANCE-Ft.)	AVERAGE G-FORCE
A	87.200	18.10	6.22
B	86.950	19.18	6.11
C	87.720	18.62	6.41
D	86.290	17.34	6.66
E	89.629	18.55	6.72
			<u>6.72</u>
			$\bar{x} = 6.42$
			S.D. = 0.265

TABLE 4.1

RESULTS FROM FIVE IDENTICAL TESTS IN WHICH
A "4,500 POUND" SCALE MODEL VEHICLE IMPACTED
A DYCON-2 CRASH BARRIER.

The results from another combination of these successful tests, in which vehicle weights and barrier materials were varied, are presented in Figures 4.3 to 4.10 inclusive. From the computer output, these graphs of both vehicle displacement and velocity versus time were plotted to obtain a comprehensive set of test results. The average deceleration was calculated for each test using the formula presented earlier in Chapter II, i.e., $G_a = \frac{V^2}{2gx}$. Then, in order that a qualitative evaluation of the barriers' performance could be made, an ideal velocity versus time curve was superimposed onto Figures 4.3 to 4.10 inclusive. These curves were obtained from the equations of rectilinear motion:

$$V = V_0 + at$$

where V = instantaneous velocity
 V_0 = initial velocity
 a = acceleration (constant)
 t = time

and

$$S = S_0 + V_0t + \frac{1}{2}at^2$$

where S = instantaneous displacement
 S_0 = initial displacement

For example, the ideal velocity vs time curve for the "4,000 pound" test vehicle in Figure 4.5 was obtained using the above equations and the following approach. As the impacting "4,000 pound" vehicle passes through the weaker front section of the barrier, the G-force developed is equal to the cushion resisting force divided by the vehicle weight or $G = \frac{24,000}{4,000} = 6$ G's. As the vehicle penetrates the stronger back section of the barrier, the cushion resisting force increases to 48,000 pounds and the G-force now becomes 12 G's. This change in G-force

produces a discontinuity in the velocity versus time curve and thus, the curve must be derived in two separate parts: V_1 , or the initial portion of the curve, and V_2 , or the final portion of the curve. The exact time that this change in slope takes place can be computed from $S = S_0 + V_0t + \frac{1}{2}at^2$ where $S = 10.5$ ft. and $S_0 = 0.0$ ft. The equations for velocity, in feet per second, versus time, in seconds, for Figure 4.5 are:

$$\begin{aligned} V_1 &= 83.92 - (6)(32.2)(t) \\ S &= S_0 + V_0t + (\frac{1}{2})at^2 \\ 10.5 &= 0 + 83.92t - (\frac{1}{2})(6)(32.2)t^2 \quad (S = 10.5 \text{ ft.}) \\ t &= 0.1515 \text{ Sec. @ } S = 10.5 \text{ ft.}) \\ V_1(\text{@}S=10.5 \text{ ft.}) &= 54.65 \text{ ft/sec} \\ &\text{and continuing} \end{aligned}$$

$$V_2 = 54.65 - (12)(32.2)(t)$$

Changing the velocity from feet per second to miles per hour, V_1 and V_2 become in equation form:

$$\begin{aligned} V_1 &= 57.22 - 131.70t \\ V_2 &= 37.26 - 263.45t \end{aligned}$$

The rest of the curves for Figures 4.3 to 4.10 inclusive were derived in a similar manner.

It is doubtful that these ideal curves could ever be obtained from an actual crash and thus, are useful only for comparison. In other words, the closer an actual velocity versus time curve matches the ideal curve, the more efficient and effective is that barrier's performance.

The first four graphs, i.e., Figures 4.3 to 4.6 inclusive, present the results of Dycon-2 barriers under the impact of a range of scale model vehicle weights. Once again, *note that these are prototype values that have been scaled from the model test results.* Also note that

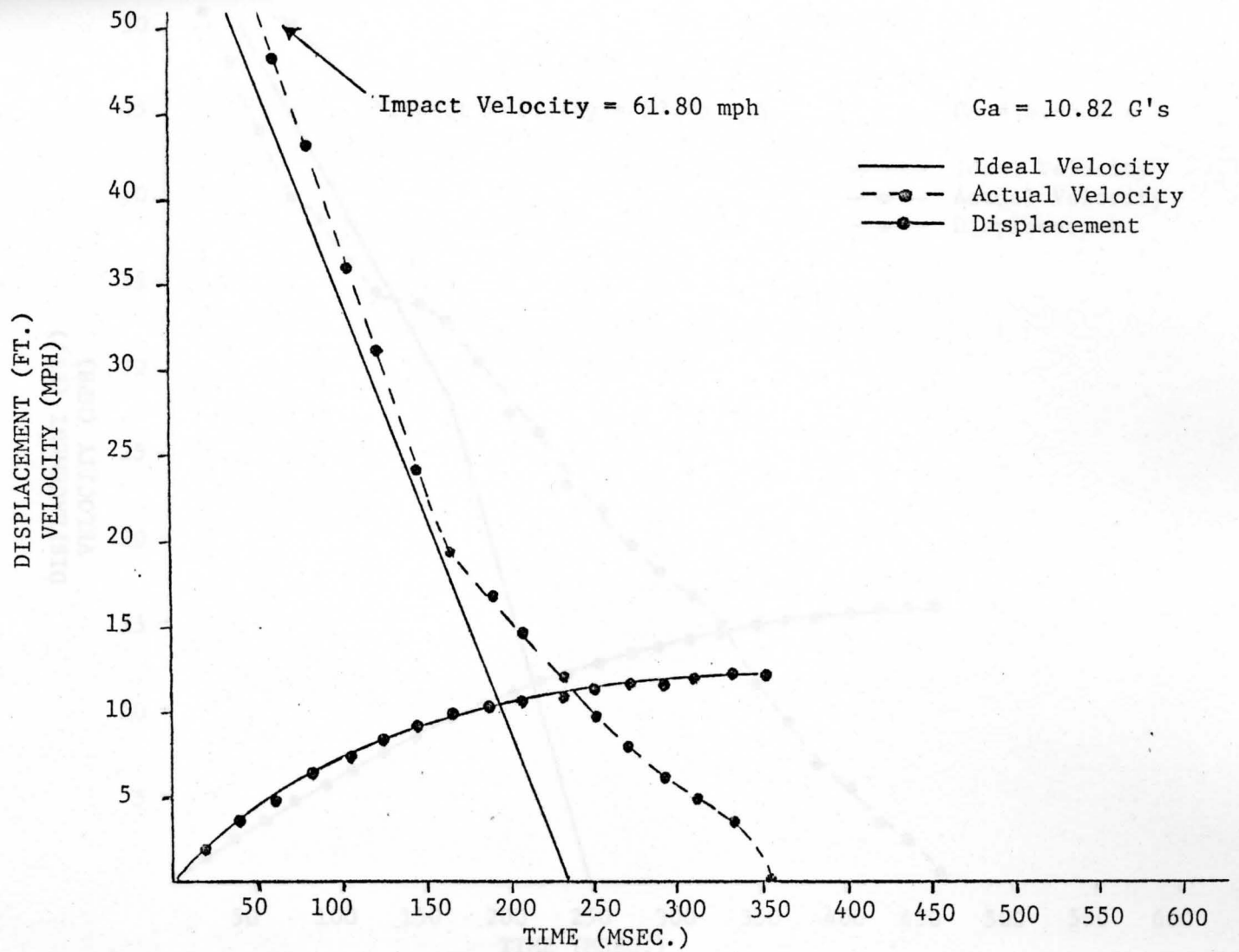


FIGURE 4.3
"2,000 POUND" CAR IMPACTING DYCON-2 BARRIER

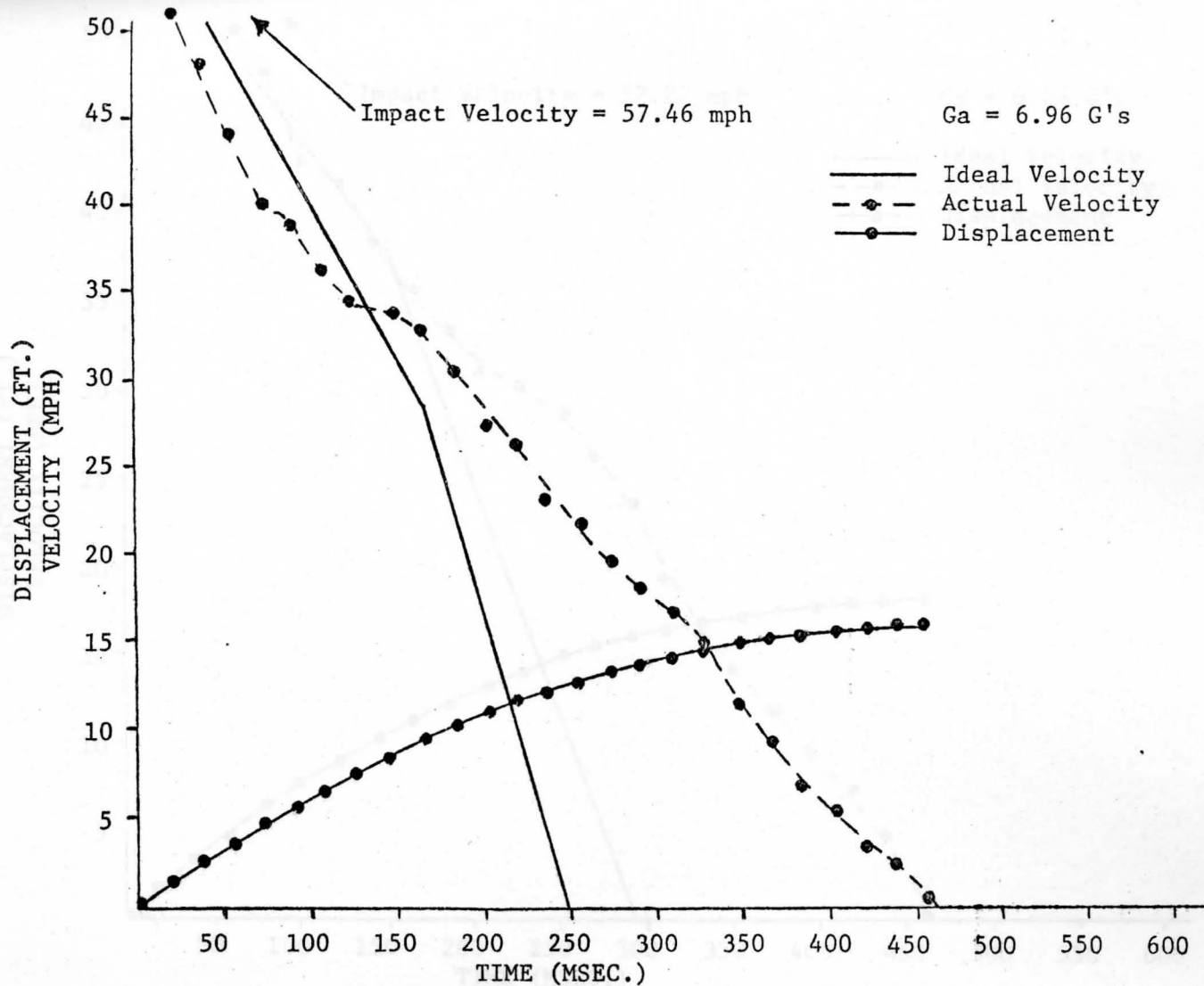


FIGURE 4.4
 "3,000 POUND" CAR IMPACTING DYCON-2 BARRIER

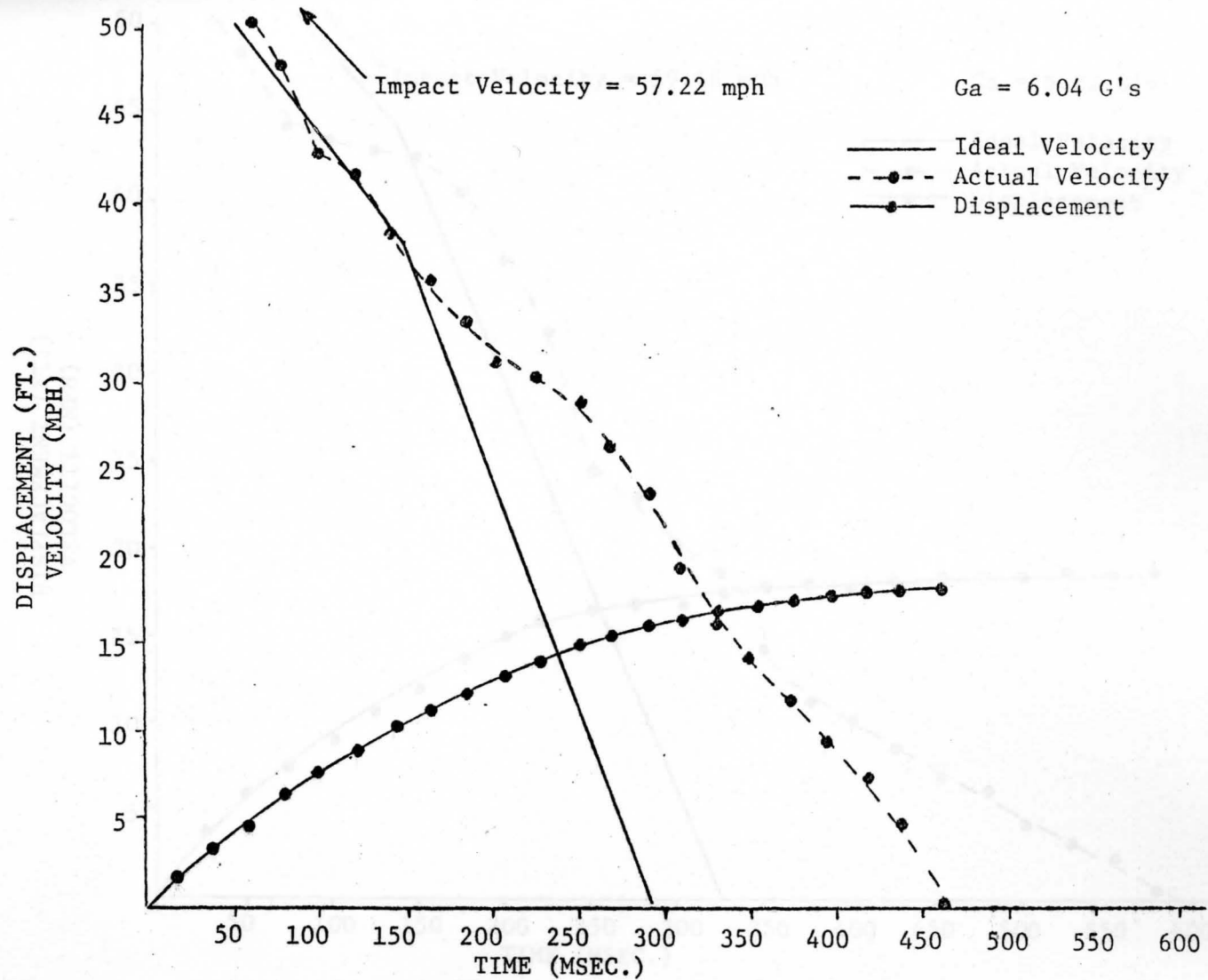


FIGURE 4.5
 "4,000 POUND" CAR IMPACTING DYCON-2 BARRIER

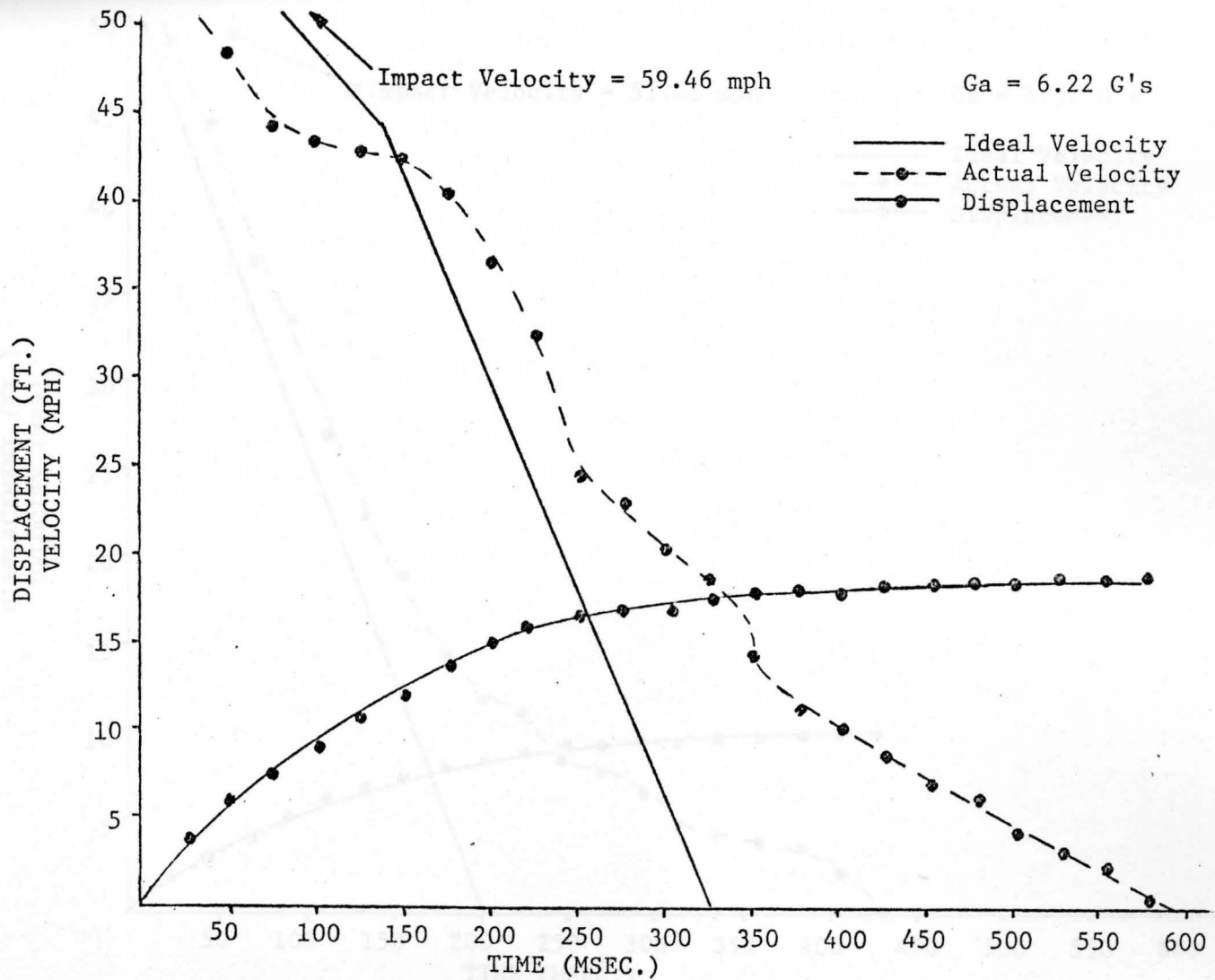


FIGURE 4.6
 "4,500 POUND" CAR IMPACTING DYCON-2 BARRIER

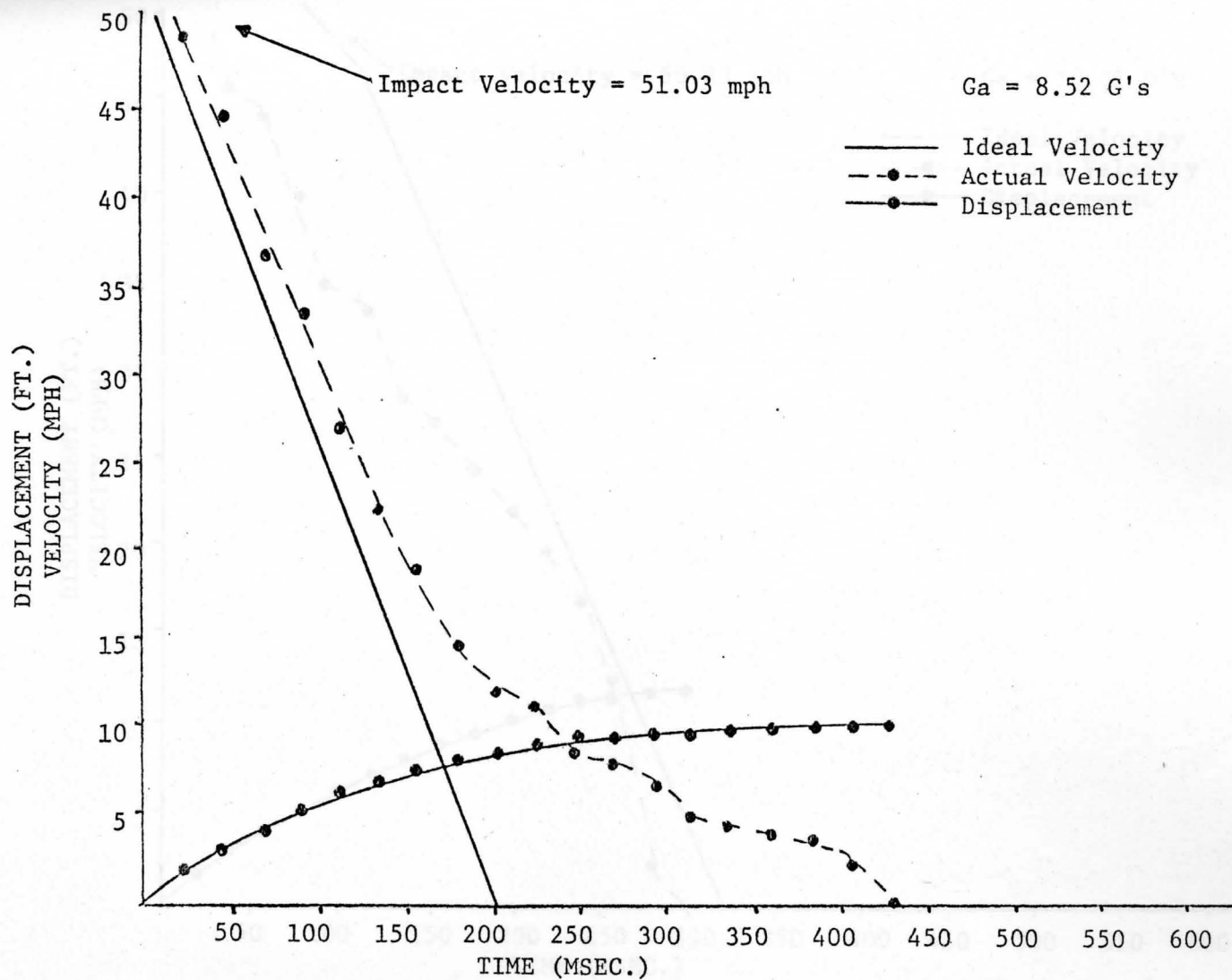


FIGURE 4.7
 "2,000 POUND" CAR IMPACTING PERLITE-4 BARRIER

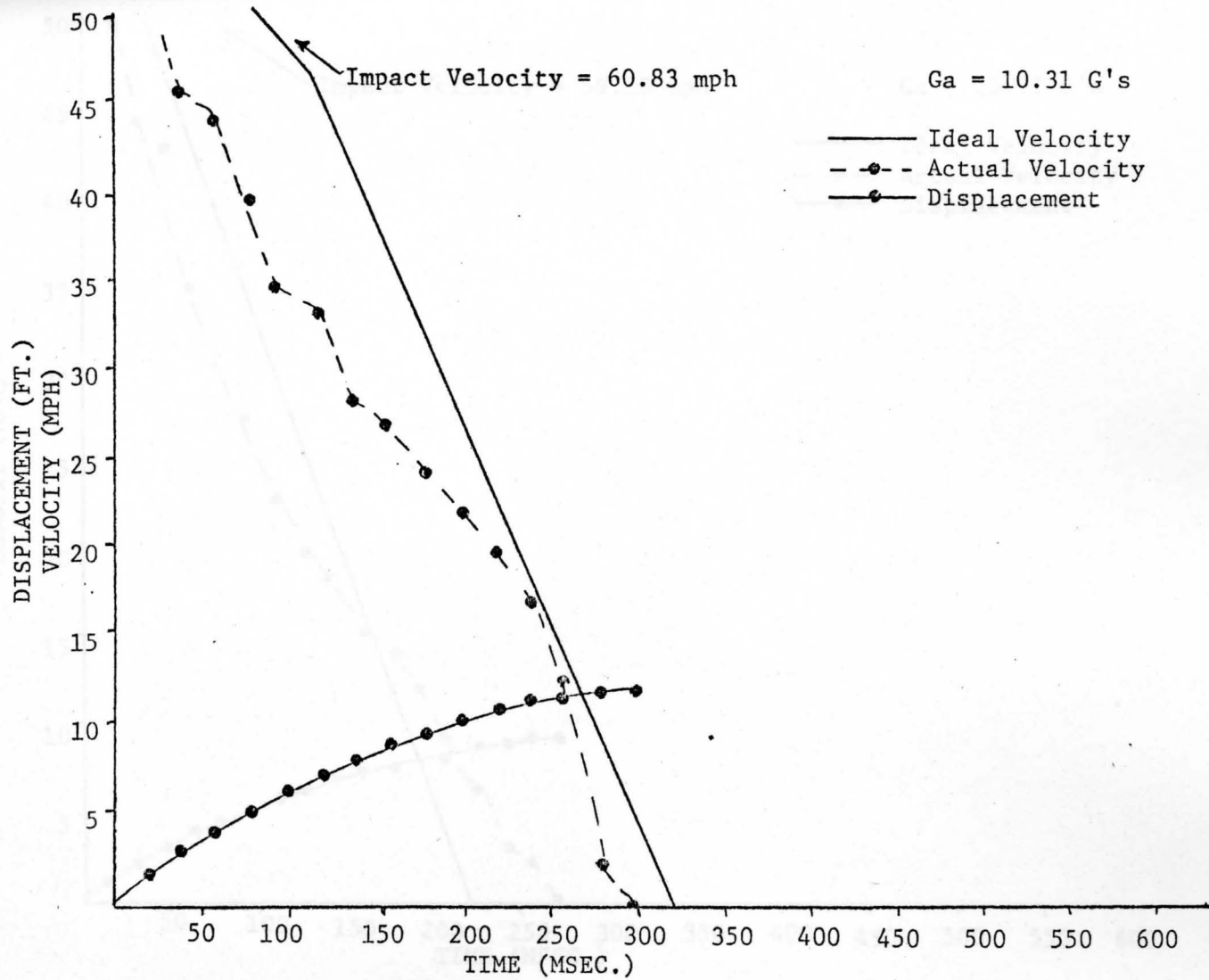


FIGURE 4.8
 "4,500 POUND" CAR IMPACTING PERLITE-4 BARRIER

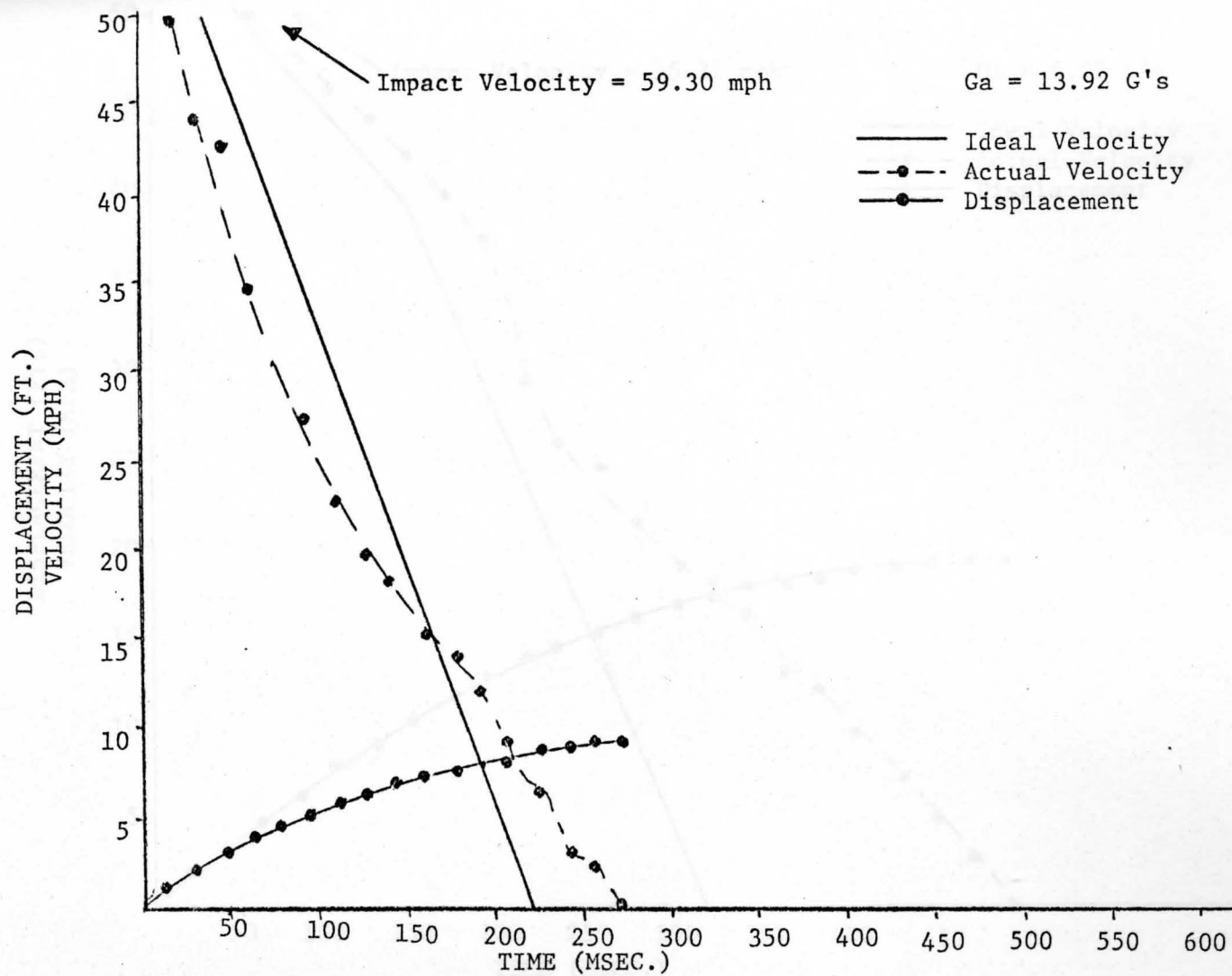


FIGURE 4.9
 "2,000 POUND" CAR IMPACTING DYCON-4 BARRIER

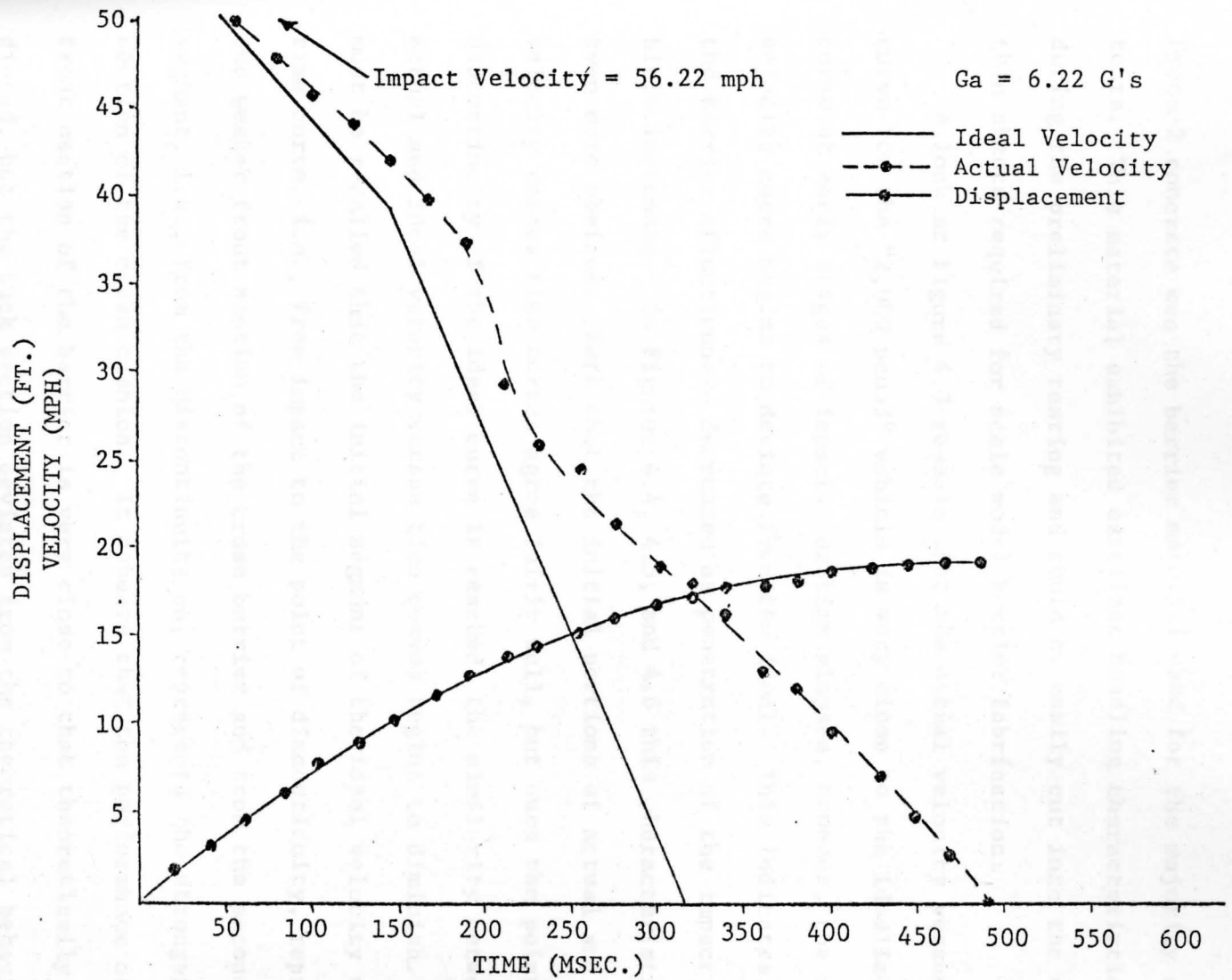


FIGURE 4.10
 "4,500 POUND" CAR IMPACTING DYCON-4 BARRIER

Dycon-2 concrete was the barrier material used for the majority of the tests. This material exhibited excellent handling characteristics during the preliminary testing and could be easily cut into the very thin sheets required for scale model barrier fabrication.

A look at Figure 4.3 reveals that the actual velocity versus time curve for the "2,000 pound" vehicle is very close to the idealized curve at early stages of impact. As time elapses, however, the actual velocity curve begins to deviate from the ideal. This indicates that the barrier effectiveness decreases as penetration of the impact vehicle increases. In Figures 4.4, 4.5, and 4.6 this characteristic is even more obvious. Note that the initial portions of actual and ideal velocity versus time curves agree fairly well, but once the point of discontinuity of the ideal curve is reached, the similarity between the actual and ideal velocity versus time curves begins to diminish. It must be recalled that the initial segment of the ideal velocity versus time curve, i.e., from impact to the point of discontinuity, represents the weaker front section of the crash barrier and from the second segment, i.e., from the discontinuity on, represents the stronger back section of the crash cushion. It appears that the performance of the front section of the barrier is very close to that theoretically predicted, but the back section deviates from the theoretical behavior. This can be attributed to the fact that the rear section of the barrier, being two modules wide, does not, in most probability, behave during collapse as efficiently, completely, and as symmetrically as the front section.

The next two graphs, i.e., Figures 4.7 and 4.8, present the

plotted data for two Perlite-4 model barriers under the impact of a "2,000" and "4,000 pound" car respectively. Perlite-4 concrete did not lend itself well to this type modeling. The material was very weak, brittle and crumbled easily. Cutting the thin sheets necessary for the model fabrication and with the required accuracy was extremely difficult. For this reason, only two Perlite-4 scale model barriers were made. In addition, it was felt that the numerous impact tests performed with Dycon-2 provided the necessary consistency of results and confidence in the design and modeling procedures that only a few Perlite tests needed to be performed. An examination of Figure 4.7 reveals the same basic type of barrier response observed earlier in Figure 4.3 for the Dycon-2 barrier. From Figure 4.8, a different type of barrier response was observed. The initial portions of the ideal and actual velocity versus time curves, which represents the weaker front section of the barrier, did not correlate well. A "4,500 pound" vehicle penetrating this section of the barrier theoretically should not have been decelerating as fast as the actual velocity versus time curve indicates. Also, as the impacting vehicle began to penetrate the stronger rear section of the barrier, it was brought to an abrupt halt resulting in very high instantaneous G-forces, i.e., 22.59 G's, and a total displacement of only 12 feet where ideally it should have been about 19 feet. This was the only barrier in which this phenomena was observed, i.e., the high instantaneous G levels within the rear section.

The next two graphs, i.e., Figures 4.9 and 4.10, present the

results from two Dycon-4 barriers under the impact of "2,000" and "4,500 pound" scale model vehicles respectively.

Before the Dycon-4 model barriers were constructed, the required wall thickness for the model barriers had to be determined. Since the mix design was not available at the time of testing, no preliminary load/deflection tests of prototype and model modules were made from Dycon-4. The wall thickness was established by fabricating several model modules using various wall thicknesses by cutting sections from a precast block of Dycon-4 that was supplied by Koppers Company, Inc. Static compression tests were conducted on these modules and the results were compared to the compression tests performed on Dycon-2 model modules. It was observed that a Dycon-4 model module having a wall thickness of $7/32$ in. produced a force-displacement curve very similar to that shown earlier in Figure 2.23. Since the scale model impact tests on Dycon-2 barriers with wall thicknesses determined from such compatible load/displacement curves proved successful, it seemed reasonable to assume that equally successful results could be obtained from Dycon-4 model barriers, i.e., those having a $7/32$ in. wall thickness. Only two Dycon-4 scale model barriers were constructed because of the limited availability of this concrete and the time-consuming nature of constructing accurate models. From the plot in Figure 4.9 it appears that in this particular impact test the average G-force was higher than the allowable 12 G's, indicating that the barrier was somewhat too rigid to safely stop the "2,000 pound" car. However, the results of the test conducted with the "4,500 pound" vehicle, shown in Figure 4.10, are almost identical to the results

from the Dycon-2 barrier under the impact of the "4,500 pound" vehicle. Although more tests would be desirable to establish a more definite response pattern, barriers constructed from this concrete appears to be feasible.

One general conclusion that can be drawn from these tests is that the weaker front sections in all of the tests conducted performed very close to that theoretically predicted. This conclusion is based upon examinations of the ideal and actual velocity versus time curves presented in Figures 4.3 to 4.10 inclusive. However, once the impacting vehicle penetrated the stronger back section of the barrier, the theory breaks down somewhat. These curves indicate that it actually takes longer to stop the impacting vehicle within this section than that predicted. The fact that this response consistently occurred indicates that there was some parameter which was not considered in the attempt to match the actual crash barrier data with theoretical predictions. As stated earlier, this missing parameter can be attributed to the inefficient response of the double wide rear section as compared to the single width of the initial portion of the barrier.

In an attempt to add some credibility to these tests, the Dycon-2 scale model barrier under the impact of the "2,000 pound" vehicle (see Figure 4.1) was compared to the results of a full scale test which was conducted by the Texas Transportation Institute.⁽²⁾ In this full scale test a crash barrier constructed from vermiculite concrete was impacted by a 2,210 pound vehicle traveling at 61.2 mph. It should be emphasized that this comparison is strictly for illustrative purposes and no attempt will be made to directly correlate the results of these

two tests. Here again, *note that the scale model test results have been scaled to prototype values by using the appropriate scale factors.* Figure 4.11 shows the full size test vehicle and its scale model counterpart. Figures 4.12 and 4.13 present selected frames from the film record of the series of events that took place upon impact. It can be seen that the mode of failure, or collapse, is very similar for both tests. Figure 4.14 presents the summarized results from these two tests. As previously stated, no direct correlation between these tests is expressed. However, the similarity between the two does add physical significance to the scale model tests and helps to bridge the gap between scale model testing and full scale verification.



FIGURE 4.11
1,210 POUND IMPACT TEST VEHICLE
AND ITS SCALE MODEL COUNTERPART

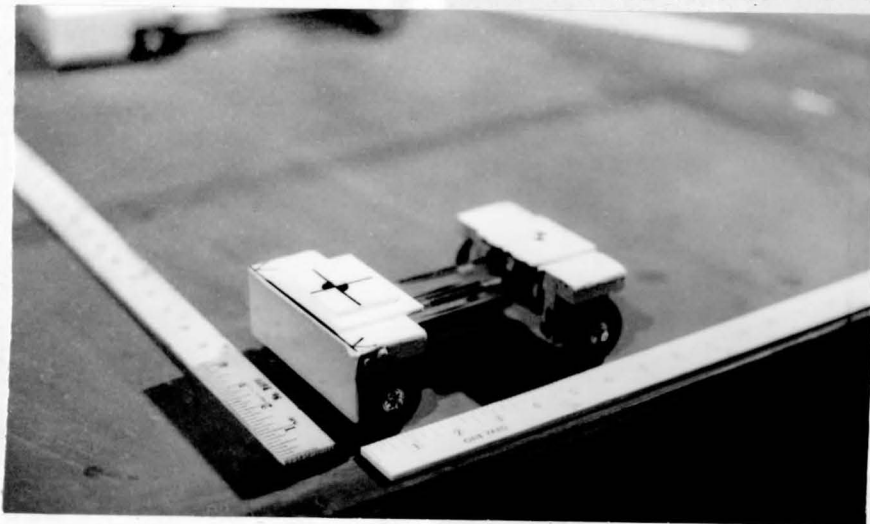
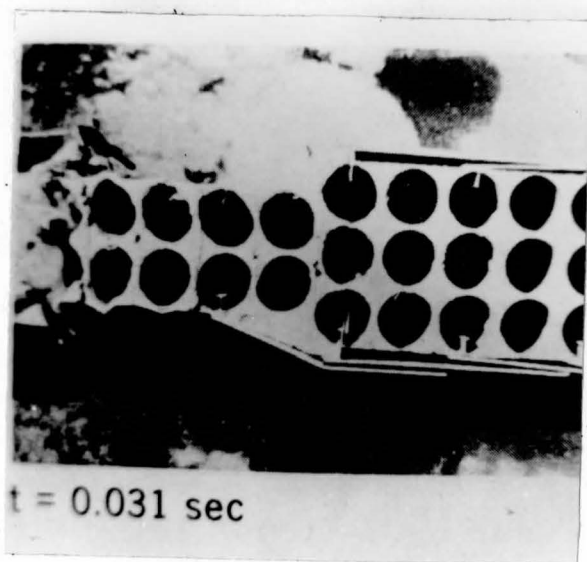
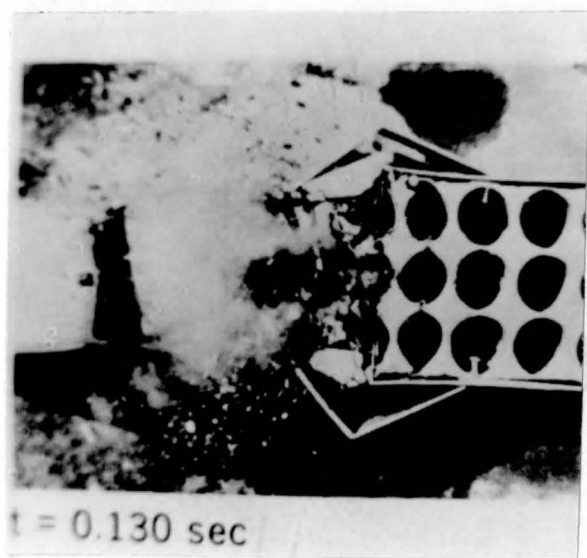
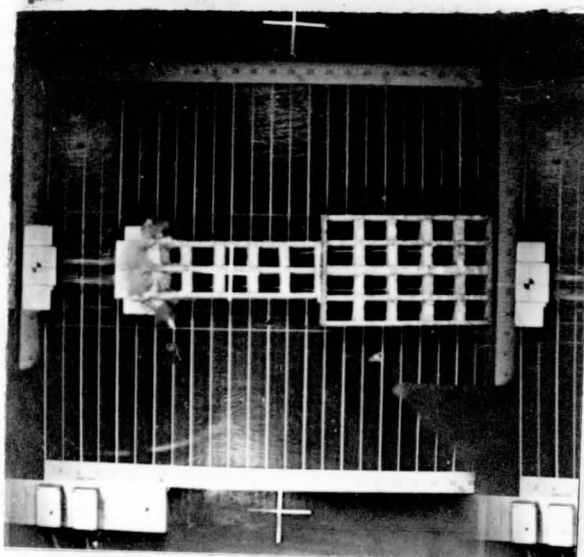


FIGURE 4.11
2,210 POUND IMPACT TEST VEHICLE
AND ITS SCALE MODEL COUNTERPART



Time = .031 Sec.



Time = .130 Sec.

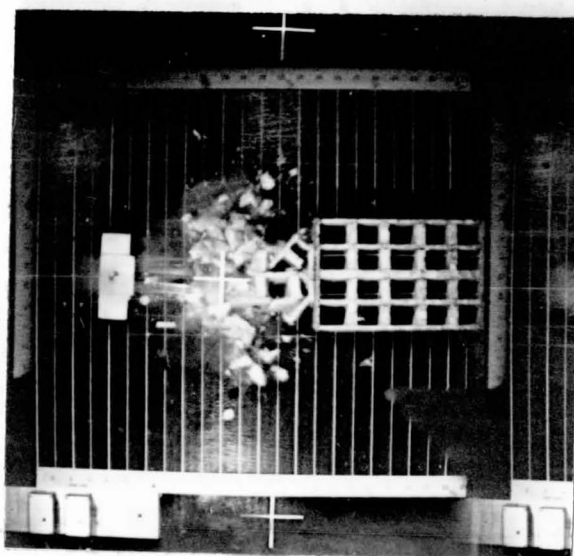
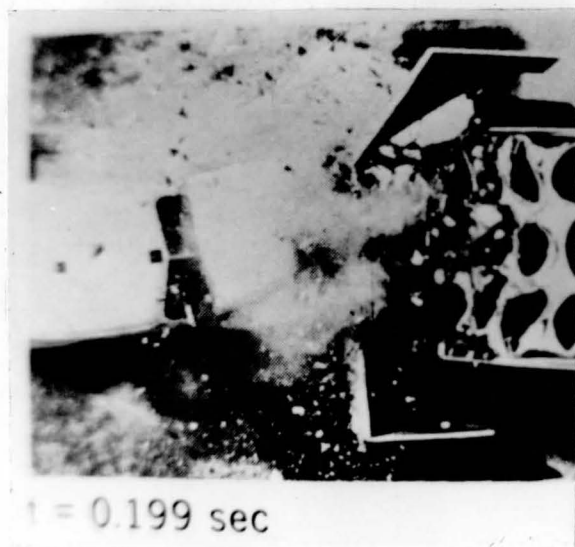
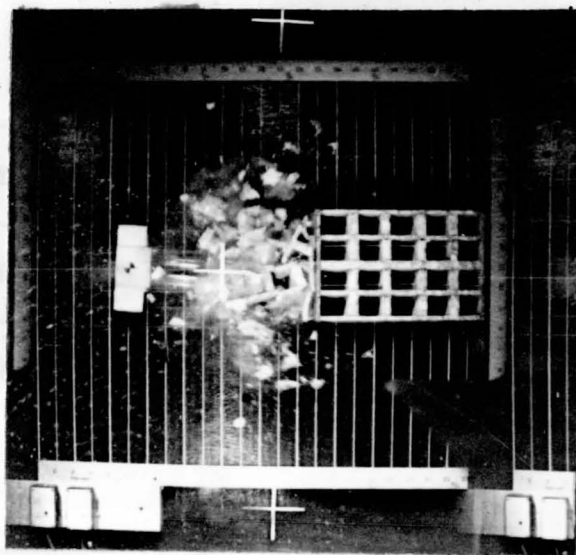


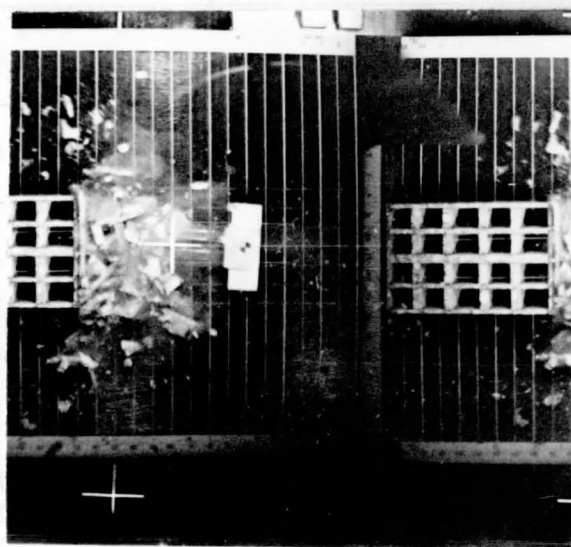
FIGURE 4.12
 SEQUENTIAL PHOTOGRAPHS OF FULL & SCALE MODEL
 2,000 POUND IMPACT TESTS



IMPACT Time = .199 Sec.



Time = .380 Sec.



Time = .354 Sec.

FIGURE 4.13
SEQUENTIAL PHOTOGRAPHS OF FULL & SCALE
MODEL 2,000 POUND IMPACT TESTS

	PROTOTYPE (a)	SCALE MODEL (b)
VEHICLE WEIGHT	2,210 POUNDS	2,000 POUNDS
BARRIER MATERIAL	VERMICULITE CONCRETE	DYCON-2 CONCRETE
IMPACT ANGLE	0°	0°
IMPACT VELOCITY	61.2 MPH	61.8 MPH
FINAL VELOCITY	0	0
AVERAGE DECELERATION	10.2 G's	10.82 G's
STOPPING DISTANCE	12.2 FT.	11.79 FT.

(a) Prototype data taken from Ref. 2.

(b) Model data has been scaled to prototype values by using the appropriate scale factors.

FIGURE 4.14
SUMMARY OF IMPACT TEST DATA FOR PROTOTYPE
AND SCALE MODEL CRASH BARRIER TESTS

CHAPTER V

CONCLUSIONS AND RECOMMENDATIONS

The utility and validity of scale model testing for use in crash attenuator design has been demonstrated numerous times before. It has been the goal of this study to apply these established techniques to the design of a full scale crash barrier without the use of expensive full scale testing. The results presented in Chapter IV are the culmination of many types of tests in which proven scaling techniques were applied to a unique material, i.e., low-density concrete, and to a unique design problem, i.e., an impact attenuator design. It is concluded that a high degree of confidence can be assigned to these results for the following reasons:

- (1) Compliance with F.H.W.A. established criteria was observed.
- (2) Scaling laws were selected with extreme care, e.g., by not scaling the impact velocity, problems arising from the strain rate sensitivity of the lightweight concrete were kept to a minimum.
- (3) Preliminary testing was accomplished to determine what effect aggregates size had on scaling.
- (4) Preliminary testing was accomplished to determine the effect of module shape on scaling.
- (5) Established barrier design procedures were followed to predict the barrier behavior upon impact.
- (6) Prototype designs were made and verified by the scale model tests.

Based upon these reasons and the agreement obtained in the impact tests, the behavior of an acceptable prototype barrier can be predicted with sufficient reliability. Because of desirable mixing, casting and

handling characteristics, favorable impact test results and excellent impact test reproducibility, the Dycon-2 crash barrier is recommended as the prototype design when built to the dimensions given in Figure 5.1. Due to undesirable cracking during handling and the difficulty encountered during the model fabrication, Perlite-4 cannot be recommended for field use. Dycon-4 cannot be fully recommended because of the limited test data available. In addition, the mix design for this concrete, developed by Koppers Company, Inc., was not available at the time of this study. The two impact tests performed on Dycon-4 models indicated that this concrete does have potential and warrants further consideration.

With the procedures and successes for the scale model testing of lightweight concrete crash barriers firmly established, further full scale testing should be undertaken to include side angle impacts along with a study of redirection panels. Installation of a prototype crash barrier at a high accident location should also be conducted to further verify the results of these scale model tests.

It is firmly believed that the low-density concrete impact attenuators provide one satisfactory solution to the menacing problem of fatal single vehicle accidents. Placement of such units at high accident locations can provide motorist protection in a safe, economical, versatile, and aesthetic manner.

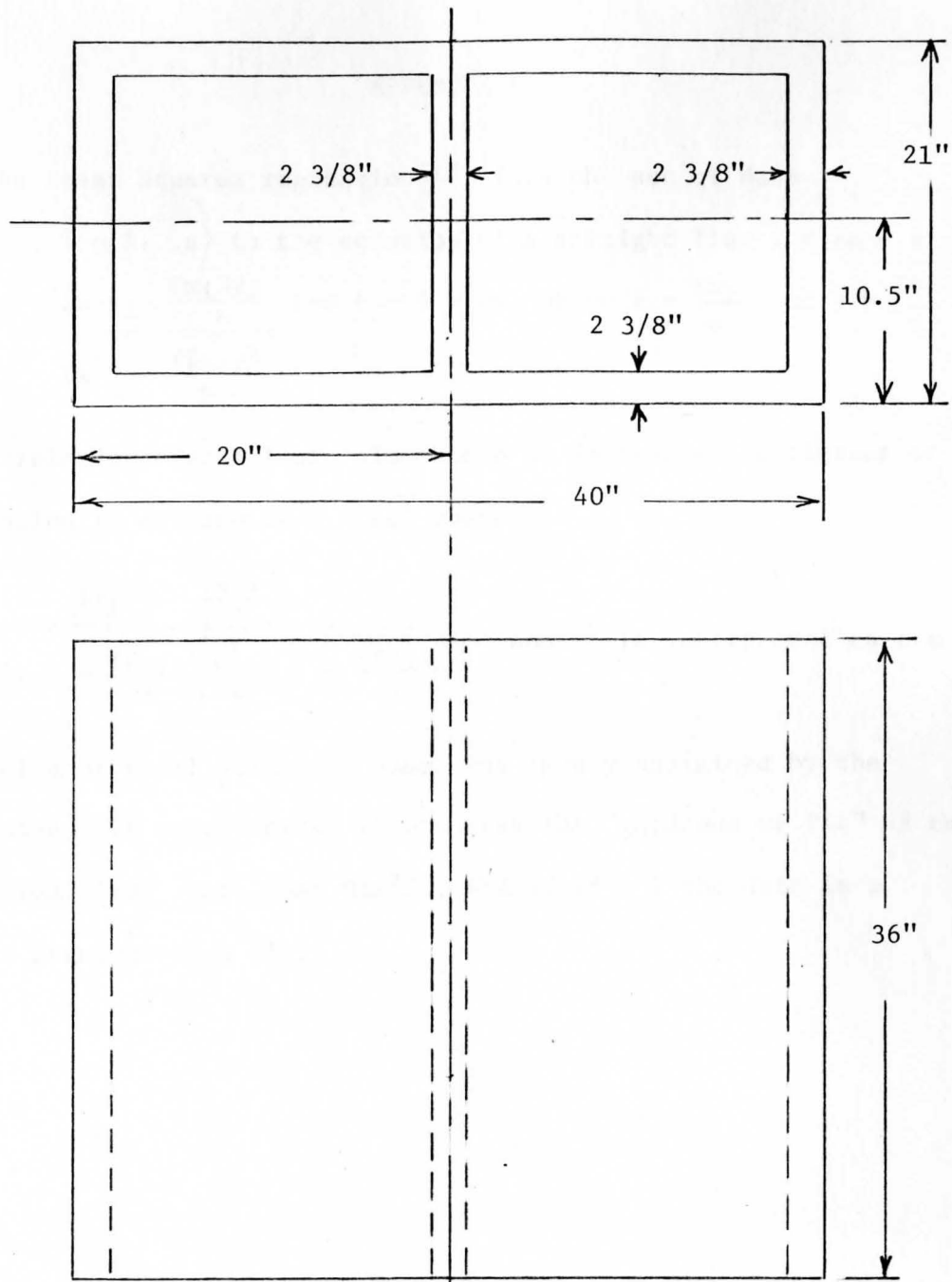


FIGURE 5.1
DIMENSIONS FOR A DYCON-2
CRASH CUSHION MODULE

APPENDIX A

The least squares regression (18)* fits the set of data $\{(x_i, y_i), i = 1 \dots n\}$ to the equation of a straight line $y = ax + b$ using $a = \frac{\sum x_i y_i - \frac{\sum x_i \sum y_i}{n}}{\sum x_i^2 - \frac{(\sum x_i)^2}{n}}$ and $b = \bar{y} - a\bar{x}$ where $\bar{x} = \frac{\sum x_i}{n}$ and $\bar{y} = \frac{\sum y_i}{n}$.

The correlation coefficient, also known as Pearson's coefficient of correlation is defined by $r = \sqrt{r^2}$ where

$$r^2 = \frac{\left[\sum x_i y_i - \frac{\sum x_i \sum y_i}{n} \right]^2}{\left[\sum x_i^2 - \frac{(\sum x_i)^2}{n} \right] \cdot \left[\sum y_i^2 - \frac{(\sum y_i)^2}{n} \right]}$$

and r^2 is interpreted as the

proportion of total variation about the mean \bar{y} explained by the regression. In other words, r^2 measures the "goodness of fit" of the regression line. Note that $0 \leq r^2 \leq 1$, and if $r^2 = 1$ the data is a perfect straight line fit.

*Number in parenthesis indicates reference cited.

APPENDIX B

The following technical specifications for the high speed motion picture camera used in this study was extracted verbatim from the camera's instruction manual.

Technical Specifications
For WF-8A Camera

This Specification sets forth the design and performance requirements for a 35 mm full-frame high speed metric recording camera with a 400 foot film capacity. Frame selected from 200 to 2,000 pictures per second, shall be regulated to provide constant speed values.

A rotary prism image motion compensator in combination with a rotating drum shutter shall produce exposures of short duration and images of high resolution and uniform density on film in continuous motion.

- 1.0 Camera Type:
High Speed Recording with 4-sided rotating prism providing motion compensation.
- 1.1 Speed Range:
200-2,000 frames per second. Operation at pre-selected values of 200, 400, 600, 800 fps in LOW range; 500, 1,000, 1,500, 2,000 fps in HIGH range speeds are selected by push button and no change in motor required. Regulation of speed within $\pm 4\%$ of pre-set value without external control accessories.
- 1.2 Frame Size:
35 mm Full Frame. Nominal .75 x 1.00 inches.
- 1.3 Film Capacity:
400 ft. Daylight loading on precision aluminum spools furnished with camera.
- 1.4 Film perforation:
Standard pitch. Either negative (ASA PH22.34-1956) or positive (ASA PH22.36-1954) perforation.
- 1.5 Acceleration to 2,000 fps in 2.1 seconds with fully loaded supply spool.

- 1.6 Start-Stop operation at 200 fps permits multiple runs. Activated by cycle switch on camera or remotely.
- 1.7 End-of-run switch automatically cuts off power to camera as film runs out.
- 1.8 Motors:
Two - One for drive and one for take-up cover complete speed range.
- 1.9 Co-Axial drum shutter rotates between rotating prism and focal plane in close proximity to aperture. This increases the effective shuttering speed and improves over-all picture quality. Effective shutter speed = $\frac{1}{4} \times \frac{1}{\text{fps}}$.
- 1.10 Fiducial Marker Projection System:
The optical axis of the camera system can be determined from the pattern of three retical marks which are optically projected into each frame. Intensity control provided which adjusts the lamp voltages. Indicator lights provided on camera front to show operation.
- 1.11 Rising Lens Board:
The lens is mounted to a plate which can be raised to change the field of view without disturbing the camera axis. A lock is provided.
- 1.12 Mounting alignment:
Two bushings in camera base have an accurate relationship to optical axis for use of locating pins. Tripod socket and four thread inserts with 310 x 16 thread.
- 1.13 Resolution: Under Optimum conditions:
40 lines/mm vertical and horizontal at center of projected frame, minimum.
40 lines/mm vertical and horizontal at edges of projected frame, minimum.
Above based on use of National Bureau of Standards test targets and 5 3/8" lens at F/5.6 with fine grain panchromatic film. (25 x reduction)
- 1.14 Rotating prism free aperture:
F/1.7 accommodation on axis.
- 1.15 Registration Accuracy:
For all medium or high frequency registration errors:
Vertical: $\pm .003$ or better at focal plane.
Horizontal: $\pm .0015$ or better at focal plane.
Test speeds are 800 and 2,000 frames/sec.

- 2.0 Power Supply:
115-125 Volts A.C., 60 cycle single phase with 30 ampere line rating and fuse level for 1,000 frames per second or less. For 1,500 and 2,000 fps, 155-175 volts A.C., 60 cycle single phase required - and a 60 amp. rating.
Available as an accessory is transformer WF365A, which provides 165 volts AC output from 220 volt AC input. Amphenol connectors designed so they cannot be interchanged, thereby preventing error.
- 2.1 Ready Light:
An electrical interlock system increases reliability by reducing possibility of operator error. Indicator lamp will light only if (a) master switch "ON", (b) transmission button engages, (c) cut-off switch closed by film under tension, (d) power cable connected, (e) camera fuse operative.
- 2.2 Magazine:
400 ft. capacity accepting heavy duty daylight loading spools. Magazine is detachable from camera body. It is loaded in attached position.
- 3.0 Focusing:
Aerial image (Parallax) method or focus-on-film.
- 4.0 Viewfinder:
A telescopic finder attached to the camera door for composition and critical through-the-lens focusing. For metric alignment and critical composing a Reflex Finder Type IV is available as an accessory. This boresight mounts between the objective lens and camera.
- 5.0 Time Marker:
Two NE51H lamps: one for event and one for time code. Marks are placed $3\frac{1}{2}$ frames ahead of aperture along edge of film and outside of perforations. Ports provided for visual check on operation of lamps.
- 6.0 Lens Mounts: FX-2 Fastax Bayonet
2 $\frac{3}{4}$ " diam. ring for 3.171" lens flange focus. This mount is one for which a number of Fastax Pro-Raptar lenses are available. Lock provided to secure lens. Heavy duty lens hood attaches to camera.
- 7.0 Optical Axis:
Vertically fixed by position of bayonet ring. Center is 7 $\frac{1}{8}$ " above camera base. Axis is

laterally positioned by two locator bushings in camera base. Bushings are on a vertical plane through optical axis.

8.0 Camera dimensions:

Size: Camera incl. magazine 22" x 25" x 12½"

Camera weight: 87 lbs.

Magazine weight: without film 23 lbs.

Shipping weight: approximately 178 lbs. in two carrying cases, packed for domestic shipment

9.0 Lens:

2" 50 mm F/2.8 (WF206A)

10.0 Film:

Eastman 4-X Negative film, 100 ft. (on spool),
35 mm K^S, No. 5224

APPENDIX C

The data presented on the following pages was extracted from the high-speed motion picture film records of the scale model impact tests. The time increment (in seconds) between film frames and the relative displacement (in inches) of the model vehicle per frame have been tabulated for all of the test results presented in Chapter IV of this report.

The raw data, as it is shown here, was transformed into usable information via the computer program listed in figure 3.3. Frame 1 was taken as the frame immediately preceding impact and the relative displacement was used to calculate the vehicle impact velocity. The remainder of the frames were used to calculate the displacement, velocity and deceleration of the vehicle after impact.

Reference has been made here to the Tables and Figures in Chapter IV generated from this data.

REFERENCE	TABLE 4.1 TEST A & FIGURE 4.6	TABLE 4.1 TEST B	TABLE 4.1 TEST C	TABLE 4.1 TEST D
TIME INCREMENT	1.791×10^{-3}	1.946×10^{-3}	1.899×10^{-3}	1.931×10^{-3}
RELATIVE DISPLACEMENT PER FRAME				
FRAME				
1	1.875	2.031	2.0	2.0
2	1.688	2.0	1.875	1.843
3	1.625	1.875	1.75	1.75
4	1.512	1.625	1.687	1.625
5	1.375	1.5	1.625	1.375
6	1.343	1.312	1.437	1.312
7	1.328	1.187	1.25	1.125
8	1.257	0.875	1.0	1.0
9	1.173	0.845	0.986	0.95
10	1.062	0.812	0.75	0.906
11	0.857	0.75	0.714	0.75
12	0.688	0.625	0.625	0.625
13	0.560	0.562	0.50	0.50
14	0.412	0.50	0.437	0.312
15	0.382	0.41	0.357	0.25
16	0.250	0.312	0.312	0.187
17	0.203	0.25	0.25	0.125
18	0.187	0.187	0.190	0.087
19	0.125	0.143	0.125	0.062
20	0.093	0.125	0.062	0.05
21	0.062	0.062	0.031	0.031
22	0.043	0.046	0.0	0.0
23	0.031	0.0		
24	0.0			

REFERENCE	TABLE 4.1 TEST E	FIGURE 4.3	FIGURE 4.4	FIGURE 4.5
TIME INCREMENT	1.453×10^{-3}	1.489×10^{-3}	1.295×10^{-3}	1.488×10^{-3}
RELATIVE DISPLACEMENT PER FRAME				
FRAME				
1	1.563	1.620	1.310	1.5
2	1.5	1.51	1.16	1.435
3	1.437	1.430	1.090	1.375
4	1.25	1.25	1.0	1.312
5	1.187	1.120	0.91	1.25
6	1.125	0.937	0.875	1.187
7	1.062	0.810	0.812	1.125
8	1.0	0.625	0.784	1.0
9	0.940	0.50	0.782	0.937
10	0.875	0.437	0.75	0.875
11	0.812	0.375	0.687	0.812
12	0.75	0.312	0.625	0.75
13	0.687	0.250	0.594	0.625
14	0.625	0.187	0.531	0.562
15	0.562	0.147	0.5	0.5
16	0.5	0.125	0.437	0.437
17	0.437	0.093	0.406	0.375
18	0.375	0.0	0.375	0.312
19	0.312		0.344	0.25
20	0.25		0.25	0.187
21	0.187		0.213	0.125
22	0.125		0.156	0.063
23	0.062		0.125	0.031
24	0.0		0.082	0.0
25			0.031	
26			0.0	

REFERENCE	FIGURE 4.7	FIGURE 4.8	FIGURE 4.9	FIGURE 4.10
TIME INCREMENT	1.601×10^{-3}	1.430×10^{-3}	1.168×10^{-3}	1.515×10^{-3}
RELATIVE DISPLACEMENT PER FRAME				
FRAME				
1	1.438	1.531	1.219	1.5
2	1.375	1.375	1.031	1.440
3	1.25	1.156	0.906	1.375
4	1.031	1.125	0.875	1.312
5	0.938	1.0	0.712	1.25
6	0.75	0.875	0.625	1.187
7	0.625	0.843	0.563	1.125
8	0.531	0.718	0.469	1.060
9	0.406	0.687	0.406	1.0
10	0.342	0.625	0.375	0.875
11	0.312	0.563	0.313	0.80
12	0.25	0.50	0.290	0.562
13	0.218	0.438	0.25	0.560
14	0.188	0.312	0.188	0.438
15	0.140	0.62	0.062	0.375
16	0.125	0.0	0.047	0.312
17	0.109			0.250
18	0.098			0.187
19	0.062			0.125
20	0.0			0.093
21				0.062
22				0.043
23				0.031
24				0.0

10. Lawrence, L. L. and Wilson, J. R., "Shock Spectrum Selection Criteria and Design", U. S. Department of Transportation, Federal Highway Administration, September 1973.

11. Covington, C., "Dynamic Energy-Absorbing Characteristics of Lightweight Versatolite Concrete", Structural Mechanics Laboratory, University of Texas, June 1961.

12. Borges, J. P., and Pereira, J., "Dynamic Model Studies for Designing Concrete Structures", American Concrete Institute Publication SP-24, pp 151-161.

13. Sushchik, Charles H., Technical and Product Information, Ford Motor Company, 1974 Representative Average Data.

14. AIA Specifications-Passenger Car, 1969, Issued 1 October 1968, Revised 3 February 1969.

REFERENCES

1. Bakos, J. D., Jr., "Development of a Low-Density Concrete Impact Attenuator", Report No. Ohio-DOT-23-73, Ohio Department of Transportation, Columbus, Ohio, 1974.
2. Ivey, D. L.; Buth, E.; Hirsch, T. J.; and Viner, J. G.; "Evaluation of Crash Cushions Constructed of Lightweight Cellular Concrete", Highway Research Record 386, 1972, pp 10-18.
3. Baker, W. E., Editor, "Use of Models and Scaling Laws in Shock and Vibration", The American Society of Mechanical Engineers Publication, November, 1963.
4. Murphy, G., Similitude in Engineering, Ronald Press Company, New York, 1950.
5. Bozich, D. J. and Kao, G. C., "A Scale Model Study of Crash Energy Dissipating Vehicle Structures", Wyle Laboratory Research Report, Huntsville, Alabama, 1969.
6. Fay, R. J. and Wittrock, E. P., "Scale-Model Test of an Energy-Absorbing Barrier", Highway Research Record 343, 1971, pp 75-82.
7. Fay, R. J. and Kaplan, M. A., "Energy-Absorbing Corrugated Metal Highway Buffer", Highway Research Record 460, 1973, pp 20-29.
8. Viner, J. G., "Recent Developments in Roadside Crash Cushions", Transportation Engineering Journal, ASCE, Vol. 98, No. TE1, Proc. Paper 8749, February, 1972, pp 71-87.
9. Kaplan, M. A.; Hensen, R. J.; and Fay, R. J.; "Space Technology for Auto-Highway Safety", Highway Research Record 306, 1969, pp 25-38.
10. Lawrence, L. R. and Hatton, J. H., "Crash Cushions Selection Criteria and Design", U. S. Department of Transportation, Federal Highway Administration, September 1975.
11. Covington, C., "Dynamic Energy-Absorbing Characteristics of Lightweight Vermiculite Concrete", Structural Mechanics Laboratory, University of Texas, June 1961.
12. Borges, J. F., and Pereira, J., "Dynamic Model Studies for Designing Concrete Structures", American Concrete Institute Publication SP-24, pp 251-263.
13. Gumushian, Charles M., Technical and Product Information, Ford Motor Company, 1976 Representative Average Data.
14. AMA Specifications-Passenger Car, 1969, Issued 1 October 1968, Revised 3 February 1969.

REFERENCES (Continued)

15. Basso, G. L., Functional Derivation of Vehicle Parameters for Dynamic Studies, National Research Council Canada, Laboratory Technical Report ST. 747, September 1974, Ottawa, Canada.
16. Ivey, D. L.; Buth, E.; Hirsch, T. J.; "Feasibility of Lightweight Cellular Concrete Vehicle Crash Cushions", Texas Transportation Institute, Technical Memorandum 505-9, January 1970.
17. Ivey, D. L.; Buth, E.; Hirsch, T. J.; "Evaluation of Crash Cushions Construction of Lightweight Cellular Concrete", Texas Transportation Institute, Technical Memorandum 505-9S, June 1971.
18. Bethea, R. M.; Duran, B. S.; Boullion, T. L.; Statistical Methods For Engineers and Scientists, New York: Marcel Dekker, Inc. 1975.

THE UNIVERSITY OF CHICAGO
LIBRARY

Master's Rimko, Robert W.
Theses
No. 145

391852
Yo. State Rimko, Robert W.
Univ. Scale model of low-
MASTER'S density concrete
THESES impact attenuators.
No. 145

DATE	ISSUED TO

391852

W. F. MAAG LIBRARY
YOUNGSTOWN STATE UNIVERSITY
YOUNGSTOWN, OHIO 44555

AUG 26 1977